Title
In vivo CRISPR screening directly targeting testicular cells.

Journal
Cell Genomics, 4(3)

Authors
Noguchi, Yuki
Onodera, Yasuhito
Miyamoto, Tatsuo
et al.

Publication Date
2024-03-13

DOI
10.1016/j.xgen.2024.100510

Peer reviewed

Cell Genomics

Technology

In vivo CRISPR screening directly targeting testicular cells

Graphical abstract

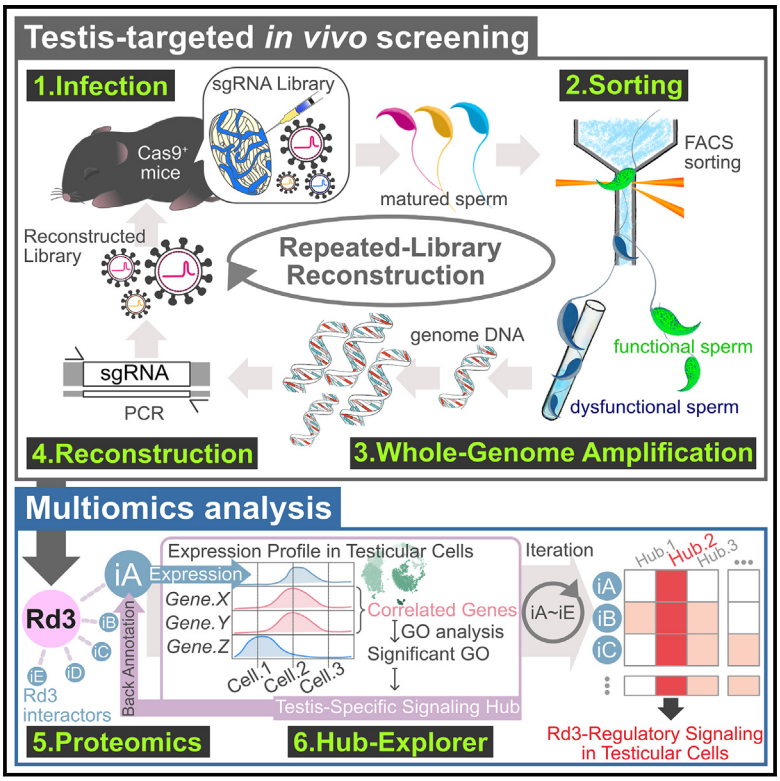

Highlights

- Application of CRISPR-Cas9 sgRNA library in testes
- Enrichment of key sgRNAs through repeated library reconstruction
- Identification of Rd3 as a factor controlling spermatogenesis
- Deduction of Rd3 signaling pathway in round spermatids with Hub-Explorer

Authors

Yuki Noguchi, Yasuhito Onodera, Tatsuo Miyamoto, Masahiro Maruoka, Hidetaka Kosako, Jun Suzuki

Correspondence

jsuzuki@icems.kyoto-u.ac.jp

In brief

Noguchi et al. developed an *in vivo* genome-wide screening system to identify factors determining spermatogenesis integrity and identified RD3 as an essential factor for spermatogenesis. They also discovered that Rd3 functions as an oxidative stress modifier in round spermatids using their originally developed computational tool, Hub-Explorer.

Noguchi et al., 2024, Cell Genomics *4*, 100510
March 13, 2024
https://doi.org/10.1016/j.xgen.2024.100510

CellPress

Cell Genomics

CellPress
OPEN ACCESS

Technology

In vivo CRISPR screening directly targeting testicular cells

Yuki Noguchi,[1,2] Yasuhito Onodera,[3] Tatsuo Miyamoto,[4] Masahiro Maruoka,[2,5] Hidetaka Kosako,[6] and Jun Suzuki[1,2,5,7,8,*]
[1]Graduate School of Biostudies, Kyoto University, Konoe-cho, Yoshida, Sakyoku, Kyoto 606-8501, Japan
[2]Institute for Integrated Cell-Material Sciences (WPI-iCeMS), Kyoto University, Yoshida-Honmachi, Sakyoku, Kyoto 606-8501, Japan
[3]Global Center for Biomedical Science and Engineering, Faculty of Medicine, Hokkaido University, N15W7 Kita-ku, Sapporo, Hokkaido 060-8638, Japan
[4]Department of Molecular and Cellular Physiology, Yamaguchi University, Graduate School of Medicine, 1-1-1 Minami-Kogushi, Ube, Yamaguchi 755-8505, Japan
[5]Center for Integrated Biosystems, Institute of Biomedical Sciences, Academia Sinica, Taipei, Taiwan
[6]Division of Cell Signaling, Fujii Memorial Institute of Medical Sciences, Institute of Advanced Medical Sciences, Tokushima University, 3-18-15 Kuramoto-cho, Tokushima 770-8503, Japan
[7]CREST, Japan Science and Technology Agency, Kawaguchi, Saitama 332-0012, Japan
[8]Lead contact
*Correspondence: jsuzuki@icems.kyoto-u.ac.jp
https://doi.org/10.1016/j.xgen.2024.100510

SUMMARY

CRISPR-Cas9 short guide RNA (sgRNA) library screening is a powerful approach to understand the molecular mechanisms of biological phenomena. However, its *in vivo* application is currently limited. Here, we developed our previously established *in vitro* revival screening method into an *in vivo* one to identify factors involved in spermatogenesis integrity by utilizing sperm capacitation as an indicator. By introducing an sgRNA library into testicular cells, we successfully pinpointed the retinal degeneration 3 (*Rd3*) gene as a significant factor in spermatogenesis. Single-cell RNA sequencing (scRNA-seq) analysis highlighted the high expression of *Rd3* in round spermatids, and proteomics analysis indicated that Rd3 interacts with mitochondria. To search for cell-type-specific signaling pathways based on scRNA-seq and proteomics analyses, we developed a computational tool, Hub-Explorer. Through this, we discovered that Rd3 modulates oxidative stress by regulating mitochondrial distribution upon ciliogenesis induction. Collectively, our screening system provides a valuable *in vivo* approach to decipher molecular mechanisms in biological processes.

INTRODUCTION

A biological phenotype is the consequence of the sophisticated interplay between gene expression and protein function in each cell.[1–3] Unveiling the molecular machinery that governs biological phenomena is crucial to understanding organisms' physiology and pathology. Over the past few decades, numerous approaches have been developed in mammalian systems to elucidate gene functions *in vivo*. One promising approach, in particular, is reverse genetics.[4–7] While single-gene knockout mice contributed significantly to understanding gene functions at an individual level,[8,9] conventional reverse genetics is unable to perturb multiple genes simultaneously within a particular tissue of each individual. In contrast, *in vivo* genome-wide screening is a powerful approach to comprehensively dissect molecular machinery underlying biological events.[10] Several studies have used CRISPR/short guide RNA (sgRNA) libraries to demonstrate *in vivo* screening of different cell types, such as cardiomyocytes,[11] neural cells,[12,13] and hepatocytes.[14,15] Most of these screening approaches used cell proliferation or locomotion as an output to enrich target cells. However, a major challenge of *in vivo* screening is to conduct biochemical-activity-based screening. Most biochemical activities are not directly related to growth, and most cells do not proliferate *in vivo*; therefore, developing a strategy to enrich target cells without cell growth is a significant issue for *in vivo* screening to overcome.

To achieve biochemical-activity-based screening without cell growth, we had established an *in vitro* screening system using a CRISPR sgRNA library, which we called "revival screening."[16] In this system, after lentiviral sgRNA introduction, target cells showing different biochemical activities are labeled with a fluorescent probe, sorted by flow cytometry based on their fluorescence intensity, and their genomic DNA (gDNA) is purified. Finally, the inserted sgRNA region is amplified from the purified gDNA by PCR to reconstitute the enriched sgRNA library. By applying this system, we successfully identified factors regulating lipid dynamics on the plasma membrane despite using dying cells, which did not exhibit growth.

Herein, we applied this system to establish an *in vivo* genome-wide screening system using mouse testes as a model tissue. To understand the factors involved in spermatogenesis, we focused

on sperm capacitation, an important event for fertilization[17–19] as a phenotypic output for functional sperms. We introduced a CRISPR sgRNA library directly into mice testes, and capacitation-defective sperms were collected by flow cytometry based on their Ca^{2+} influx, a well-known biochemical activity of capacitation.[20–23] Through *in vivo* revival screening, we identified retinal degeneration 3 (Rd3), whose defect causes Leber congenital amaurosis (LCA) type 12[24–26] as a factor involved in spermatogenesis. Through these achievements, we demonstrated that our *in vivo* genome-wide screening approach can be widely applicable to biochemical-activity-based screening in the future.

DESIGN

We designed a testes-targeted *in vivo* CRISPR screening system, marked by four key achievements: (1) introduction of an sgRNA library into male germ cells via Sendai virus fusion (SVF) protein-coated lentivirus,[27,28] (2) evaluation of spermatogenesis integrity by measuring levels of sperm Ca^{2+} influx at a high signal-to-noise ratio,[20–23] (3) efficient readout of sgRNA sequences from a small number of sperms using primase-based whole-genome amplification (pWGA),[29] and (4) enrichment of critical sgRNAs through repeated library reconstitution as part of our advanced revival screening method.[16]

Hub-Explorer is a computational analysis tool designed to unravel key regulatory pathways in particular cell types. This tool adeptly combines two fundamental components: a gene co-expression network (GCN) and Gene Ontology (GO) terms. To perform this analysis, Hub-Explorer necessitates three essential inputs: (1) a gene expression matrix, (2) a list of genes of interest, and (3) annotation files that establish connections between gene symbols and UniProt IDs. In our study, we utilized single-cell RNA sequencing (scRNA-seq) data from testicular cells as the gene expression matrix and proteome-derived data of Rd3 interactors as the list of genes of interest. For generating the GCN, Spearman's correlation coefficient ($\rho > 0.8$) was utilized. Subsequently, a GO analysis was conducted for each gene within the GCN. We classified genes within the GCN by assessing the Jaccard similarity index of their GO term annotations. The final step involved pinpointing shared GO terms among these genes, enabling us to delineate the core regulatory pathways.

RESULTS

Establishment of *in vivo* genome-wide screening

To develop a method for *in vivo* genome-wide screening using mice testes, we first established the technical basis of the screening system, by focusing on four distinct components, as illustrated in Figure 1A. Initially, efficient viral injection methods were determined by introducing lentiviruses into testes. First, lentiviruses encoding EGFP with the mitochondrial signal sequence (9×10^7 infectious titer unit [IFU]/mL) were introduced into the testes of 11 postnatal day (PND) mice according to previously reported methods[30,31] such as seminiferous tubular injection and interstitial injection. Successful infection was confirmed with seminiferous tubular injection but not with interstitial injection (Figure S1A). Next, to determine the effective virus titer, two different titers of lentiviruses (2.5×10^6 and 9×10^7 IFU/mL) were introduced into mice testes by seminiferous tubular injection. Lentivirus infectivity was found to increase in a titer-dependent manner (Figure S1B). However, most of the infected cells were thought to be Sertoli cells because the EGFP signal showed a broad spreading pattern from the basal to the apical side[32] (Figure S1B), and this signal co-localized with the anti-vimentin antibody signal (Figure S1C). These results are consistent with previous studies[30–32] and suggested that not only viral titer but also virus tropism are critical factors for successful infection. Recently, a highly selective lentivirus for male germ cells was developed using SVF proteins.[27,28] Utilizing this system, we endeavored to deliver lentiviruses into male germ cells. Initially, we transfected plasmids carrying SVF protein and viral components into HEK293T packaging cells. After transfection, sodium butyrate was added to enhance gene expression for generating high-titer lentiviruses. SDS-PAGE of the purified lentiviruses, followed by Coomassie brilliant blue staining, was able to detect the SVF protein consistent with its reported size[33] (Figure S1D). Based on these improvements, we successfully generated a high-titer SVF lentivirus (3×10^7–3×10^8 IFU/mL). Microscope analysis showed effective viral introduction into $Gcna1^+$ germ cells[34] 1 week after infection (Figures 1B and S1E). Flow cytometry analysis also confirmed that $54.2\% \pm 2.67\%$ of $Cdh1^+$ type A spermatogonia (SPGs)[35] were infected by TagBFP-encoded lentivirus (Figure S1F), and TagBFP expression was sustained for 8 weeks (Figure S1G). We next examined sgRNA on-target efficiency to evaluate whether Cas9 was functional in the germ cells of CRISPR-Cas9 knockin mice. Lentivirus encoding sgRNA against Rosa26 was injected into testes via seminiferous tubule, and insertions or deletions (indels) at the Rosa26 locus in $Basigin\ (BSG)^+$ germ cells[36] were confirmed by Sanger sequencing (Figure 1C). Knockout effects of sgRNA against Gcna1 were also shown at the protein level in $Plzf^+/Sall4^+$ type A SPGs[37,38] and primary spermatocytes with 46 double-structured chromosome[39] using flow cytometry (Figure 1D). These results demonstrated successful targeting by lentiviral sgRNAs in germ cells.

Since we successfully introduced lentiviruses into testicular cells and achieved genetic perturbation for *in vivo* genome-wide screening, we aimed to determine a screening target to elucidate spermatogenesis quality, which could be analyzed by flow cytometry. Among various indicators to evaluate spermatogenesis, we decided to focus on the capacitation of mature sperms, which is a crucial process for fertilization[17–19] and reflects spermatogenesis quality.[40–42] Among the several processes associated with capacitation, Ca^{2+} influx is widely known as a driving force for capacitation.[20–23] When Ca^{2+} influx was examined by flow cytometry using the Ca^{2+} indicator Fluo-4 AM, a drastic intracellular Ca^{2+} increase was observed under capacitation conditions (Figure 1E). Scanning electron microscopy (SEM) analysis of sperm morphology was also performed to validate capacitation capability. As expected, we observed an acrosome-reaction-derived morphological change in the sperm head, which appeared after the end of capacitation[43] (Figure S1H). In summary, these fine-tuned experimental conditions

CellPress
OPEN ACCESS

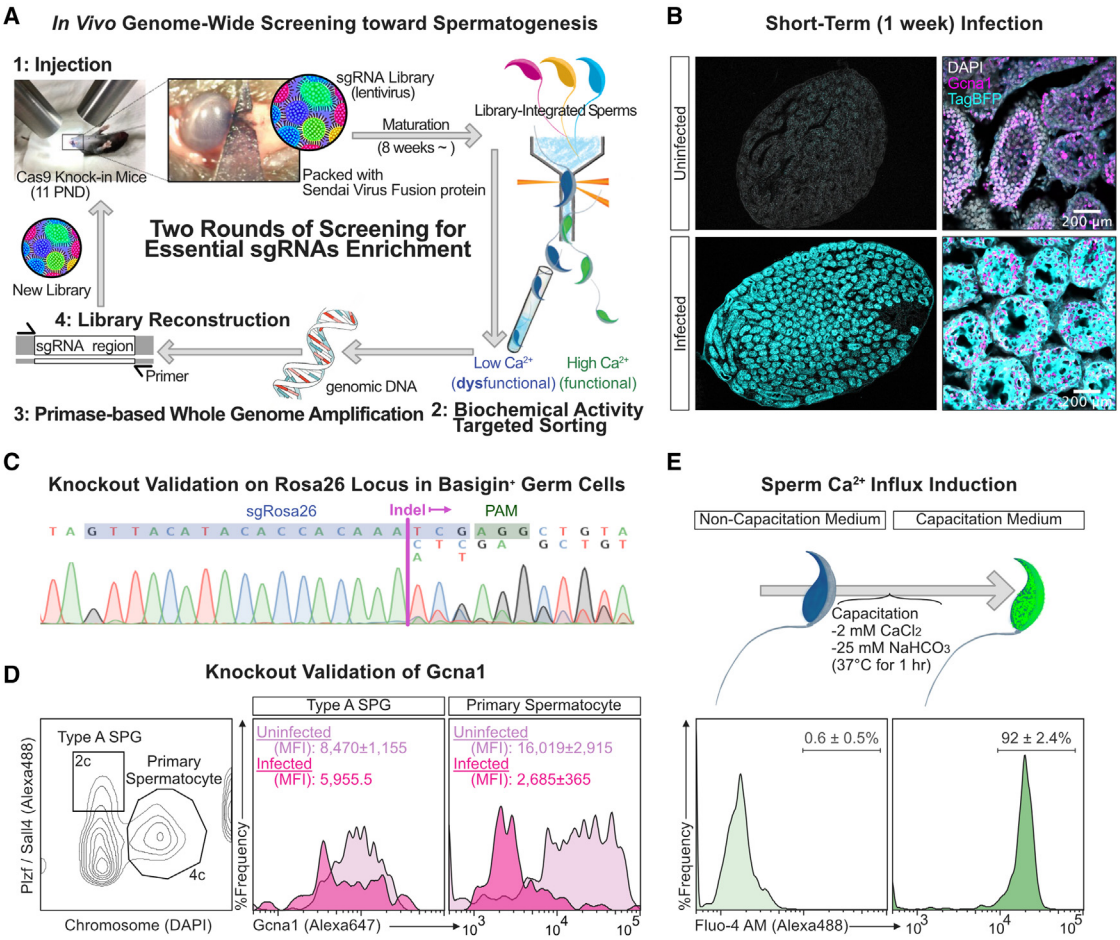

Figure 1. Establishment of *in vivo* genome-wide screening

(A) Experimental scheme of *in vivo* genome-wide screening toward spermatogenesis.

(B) Evaluation of short-term infection efficiency. Lentivirus encoding TagBFP was injected into 11 PND mice testes. One week later, cryo-sectioned testes were stained with anti-TagBFP (cyan) and anti-Gcna1 (magenta) antibodies and DAPI (white), followed by confocal microscopy analysis. Top: virus uninfected; bottom: virus infected. Left: macroscale; right: microscale. Scale bar: 200 μm.

(C) Sanger sequencing analysis against Rosa26 region in Basigin (Bsg)$^{+}$ germ cells. Lentivirus encoding sgRosa26 and TagRFP was introduced into 11 PND mice testes. Ten days later, male germ cells were stained with anti-Bsg antibody. TagRFP^{+} and Bsg^{+} germ cells were sorted for gDNA extraction. Indel start position was detected by CRISP-ID, shown as an orchid-colored line. Experiment was repeated twice.

(D) Gcna1 knockout (KO) efficiency evaluation. Lentivirus encoding sgGcna1 and TagBFP was introduced into 11 PND mice testes. One week later, dissociated testes were stained with anti-Plzf, anti-Sall4, and anti-Gcna1 antibodies and DAPI. Analyzed cells are shown on the left. Gcna1 signal intensity was evaluated by median fluorescent intensity (MFI) as mean ± SD. Middle: type A spermatogonia (Plzf^{+}/Sall4^{+}); right: primary spermatocyte (4 chromosomes). Light orchid: uninfected cells; dark orchid: infected cells. Infected samples in type A spermatogonia were analyzed twice (n = 2), and the others were analyzed three times (n = 3).

(E) Evaluation of sperm Ca^{2+} influx. Adult mice sperms were capacitated (top; see the STAR Methods) and stained with Fluo-4 AM and PI. Fluo-4 AM signal in PI-negative region was analyzed. Bottom left: non-capacitated sperms; bottom right: capacitated sperms. Experiments were repeated three times (n = 3), and Fluo-4 AM-positive populations were shown as mean ± SD.

would enable us to perform genome-wide screening using testes.

Enrichment of essential sgRNAs associated with spermatogenesis

As we had successfully established a method to introduce a lentiviral sgRNA library into germ cells, we next validated genome-wide coverage in type A SPGs by administering the GeCKO-v2 mouse sgRNA pool B library, consisting of 62,804 unique guide sequences, into the testes of Cas9 knockin mice.[44] Three days after lentiviral library injection, Plzf^{+} type A SPGs were sorted, and sgRNAs integrated into the gDNA of these cells were sequenced by next-generation sequencing (NGS). To statistically evaluate our screening result, we considered the following two aspects: (1) the distribution of sgRNA counts and targeted genes and (2) the profile of sgRNA counts per gene (detailed in the STAR Methods). From the result, we confirmed that there was no experimental bias in our screening (Figures S2A–S2D).

As for the evaluation of library coverage, sgRNA clone coverage analysis showed a 42.3% coverage ratio in three testes

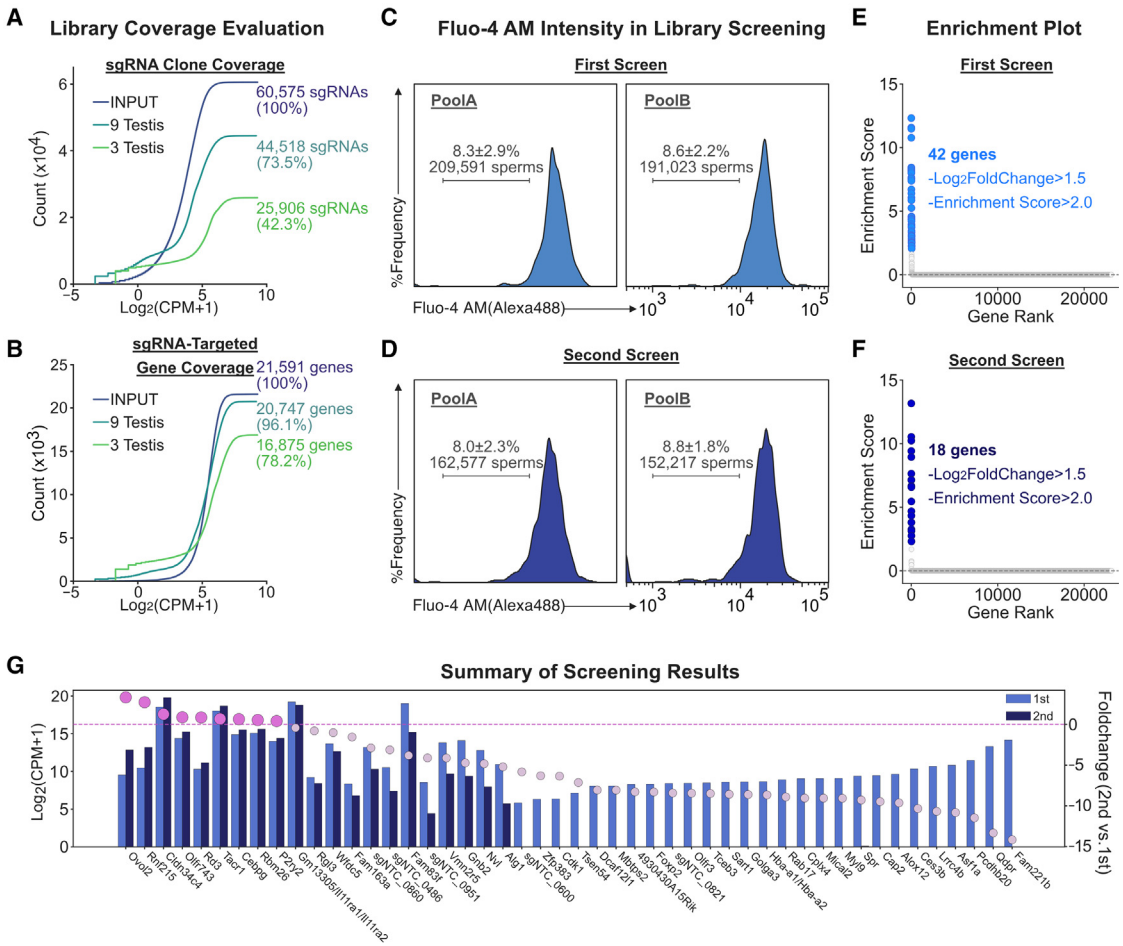

Figure 2. Enrichment of essential sgRNAs associated with spermatogenesis

(A and B) Library coverage evaluation. Pool B GeCKO-v2 sgRNA library containing 62,804 sgRNAs was introduced into 11 PND mice testes. Three days later, dissociated testes were stained with anti-Plzf and DAPI to sort Plzf$^+$ type A spermatogonia for gDNA extraction. The amplified sgRNA regions were sequenced with the next-generation sequencing (NGS). The sgRNA clone coverage is shown in (A) and the sgRNA-targeted gene coverage is shown in (B). sgRNAs from are from input (blue), 9 testes (dark green), and 3 testes (light green). x axis: the sgRNA count (=$\log_2$(CPM + 1)); y axis: the cumulative sgRNA count.

(C and D) Sorting diagram of Fluo-4 AM-negative sperms. Left column: pool A; right columns: pool B. (C) First screen. (D) Second screen.

(E and F) Significant gene enrichment. Significant genes were extracted above $\log_2$ fold change = 1.5 and enrichment score = 2.0. Candidates in the first library are shown as light blue dots (E) and those in the second library are shown as dark blue dots (F). Enrichment score was calculated as described in the STAR Methods.

(G) Enriched candidate genes. Light blue bar: first screening; dark blue bar: second screening. Count shown as $\log_2$(CPM + 1). Fold change (count of second screening/first screening) is shown as colored dots (orchid: enriched genes; light orchid: non-enriched genes).

(Figure 2A). An additional six testes (total: nine testes) were further examined, and the sgRNA clone coverage was 73.5% (Figure 2A). The sgRNA-targeted gene coverage was also analyzed in three testes and nine testes. The sgRNA-targeted gene coverage in three testes was calculated to be 78.2% (Figure 2B). In nine testes, the sgRNA-targeted gene coverage was 96.1% (Figure 2B). In addition, this tendency was not altered even 1 week after infection (sgRNA clone coverage: 67.8% [Figure S2E]/sgRNA-targeted gene coverage: 94.2% [Figure S2F]), suggesting that the genome-wide coverage of sgRNAs in the testes was sufficient for screening.

Based on the obtained coverage ratio in testes, we introduced the GeCKO-v2 mouse sgRNA library into Cas9 knockin mice testes at 11 PND: the pool A and pool B libraries were infected into twelve testes during the first screen and into eight testes during the second screen. Eight weeks after infection, mature sperms, which developed from the infected germ cells, were obtained from the cauda epididymis, incubated with capacitation buffer, stained with Fluo-4 AM and propidium iodide (PI), and finally applied to cell sorting using flow cytometry. In the first round of screening, we sorted 209,591 Ca^{2+} uptake-negative sperms (corresponding to 8.3% ± 2.9% of input) from testes infected with virus from the pool A library and 191,023 Ca^{2+} uptake-negative sperms (corresponding to 8.6% ± 2.2% of input) from testes infected with virus from the pool B library (Figure 2C). After sorting, gDNA was purified from the sorted sperms and applied to pWGA[29] (see the STAR Methods). Using the amplified gDNA, the integrated sgRNA region was then amplified by PCR

and inserted into lentiviral vectors. The reconstituted sgRNA library was then applied to the next round of screening so that false positive hits could be eliminated. In the second round of screening, we sorted 162,577 Ca^{2+} uptake-negative sperms (corresponding to 8.0% ± 2.3% of input) from the enriched pool A library testes and 152,217 of Ca^{2+} uptake-negative sperms (corresponding to 8.8% ± 1.8% of input) from the enriched pool B library testes (Figure 2D). After gDNA purification from the sorted sperms and pWGA using the purified gDNA, the integrated sgRNA region was amplified by PCR. The sgRNAs from the first and second rounds of screening were then analyzed by NGS and mapped to reference sequences.

For NGS analysis, we developed the enrichment score (ES) (see STAR Methods) to precisely analyze detected sgRNAs while maintaining correlation between $\log_2$ fold change and ES at a significant value range (ES > 2.0 and $\log_2$ fold change > 1.5) (Figures S2G and S2H). According to the ES, we identified eighteen sgRNA-targeted genes in the second round of screening from forty-two sgRNA-targeted genes nominated in the first round of screening (Figures 2E and 2F). When we compared these sgRNAs derived from the second round of screening to those from the first round, we observed a significant enrichment of genes involved in reproduction, such as copulation and mating (Figure S2I). Notably, we observed an increase in the read counts of nine sgRNA-targeted genes and a decrease in all non-targeting sgRNAs in the second round of screening (Figure 2G). These results suggest that our *in vivo* genome-wide screening approach successfully enriched sgRNAs that regulate spermatogenesis.

Rd3 is an essential spermatogenesis factor identified through small-scale functional screening

In order to further narrow down the candidates, we analyzed gene expression and the effect of gene disruption on testis weight, sperm numbers, and Ca^{2+} influx (Figure 3A). We first analyzed the transcriptome dataset obtained via Bgee.[45] The transcriptome analysis indicated that the expression of seven genes (*Ovol2*, *Rnf215*, *Cldn34c4*, *Rd3*, *Cebpg*, *Rbm26*, and *P2ry2*) out of the nine candidates was observed in adult testes (Figure 3B). Further quantitative RT-PCR (RT-qPCR) using 8 week testis RNA also confirmed this result (Figure S3A). One of the nine candidates, *Olfr743* was found to be expressed at 5 and 6 weeks but decreased at 8 weeks (Figure S3B). Another candidate, *Tacr1*, was not expressed in testicular cells, suggesting that the false positive rate was one-ninth (Figure S3C).

Based on the gene expression analysis, a small-scale short hairpin (sh)RNA screening against the seven candidates, selected based on gene expression level, was performed to validate the function of each gene. Firstly, the efficiency of each shRNA-mediated knockdown was validated in cell lines using RT-qPCR, confirming a reduction in RNA expression to 34.4% ± 14.7% (Figure S3D). Subsequently, the validated lentiviral shRNAs were injected into testes at 11 PND via their seminiferous tubules. The lentiviral infection efficiency of each shRNA into testes was determined by the expression of fluorescent proteins in Bsg^{+} germ cells,[36] which were isolated from the dissociated testes after measuring testicular weight. From this, the average infection efficiency was found to be 24.9% ± 15.3% (Figure S3E). As for the phenotypic effect, knockdown of *Ovol2*, *Cldn34c4*, *Rd3*, and *P2ry2* led to a decrease in testicular weight (Figure 3C). Among these, sh*Rd3* decreased testicular weight most significantly. Considering that sh*Rd3*-encoded lentivirus had the lowest infection efficiency, silencing of *Rd3* may affect testicular cell survival the most. In addition, sperm numbers were decreased after *Cldn34c4*, *Rd3*, and *P2ry2* knockdown (Figure 3D). Among the seven candidates, *Rd3* knockdown decreased Ca^{2+} influx significantly (Figures 3E, 3F, and S3F–S3H). These results strongly indicated that *Rd3* was the most promising factor contributing to spermatogenesis among the identified genes.

Round spermatid is the specific cell type with high Rd3 expression in testis

RD3 has been reported as an essential factor for retinogenesis, specifically through the regulation of retinal guanylyl cyclase 1/2 in the outer segment of the retina, and loss-of-function mutations in *RD3* cause LCA type 12.[25,26,46] Although one report suggested that RD3 is expressed in human testes,[47] the role of mouse Rd3 in spermatogenesis remains unknown. To elucidate the molecular functions of Rd3 in spermatogenesis, we first investigated Rd3 expression in testes using both transcriptome and histology approaches. We utilized the tissue-wide transcriptome dataset, also used in Figure 3B, and found that *Rd3* is highly expressed in the retinal neural layer and testes (Figure 4A). Since *Rd3* is highly expressed in the testes, we next utilized the testicular scRNA-seq dataset[48] to identify *Rd3*-expressing cell types. Based on the scRNA-seq results, the cell population was grouped into seven discrete clusters (Figure 4B). When *Rd3* expression was compared among these clusters, it was found to be increased during spermatogenesis and, in particular, became the highest in the latter stage of round spermatid (Figure 4C), when *Acrv1*[49] and *Spaca4*[50] were strongly expressed (Figure S4A). In addition, retinal scRNA-seq analysis also showed that rod and cone cells had the highest *Rd3* expression among the twelve distinct retinal cell types[51] (Figures S4B and S4C). Comparative transcript isoform analysis between the testis and retina using other transcriptome datasets (Accessions: SRR823506 and SRR342458[52]) revealed that the 5′ UTRs of *Rd3* in these two tissues are distinct, implying that *Rd3* translational regulation differs between the testis and retina (Figure S4D). We then validated *Rd3* expression by RT-qPCR analysis and confirmed that *Rd3* expression starts to increase 3 weeks after birth, when round spermatids increase in number,[48] and reaches a maximum at 7 weeks (Figure 4D). This result was verified by RT-PCR with different amplification cycles (Figure 4E). Hybridization-chain-reaction-based fluorescent *in situ* hybridization and immunohistochemistry using adult mice testes showed that Rd3 mRNA and protein were detected in $Acrv1^{+}$ round spermatids[49] and lectin PNA^{+} whole spermatids[53] (Figures 4F and 4G).

Identification of ciliogenesis-oriented Rd3-mitochondria axis by Hub-Explorer analysis

To uncover the function of Rd3 in round spermatids in testes, we first attempted to perform proteomics analysis to give us insights into the function of Rd3. However, conducting *in vivo*

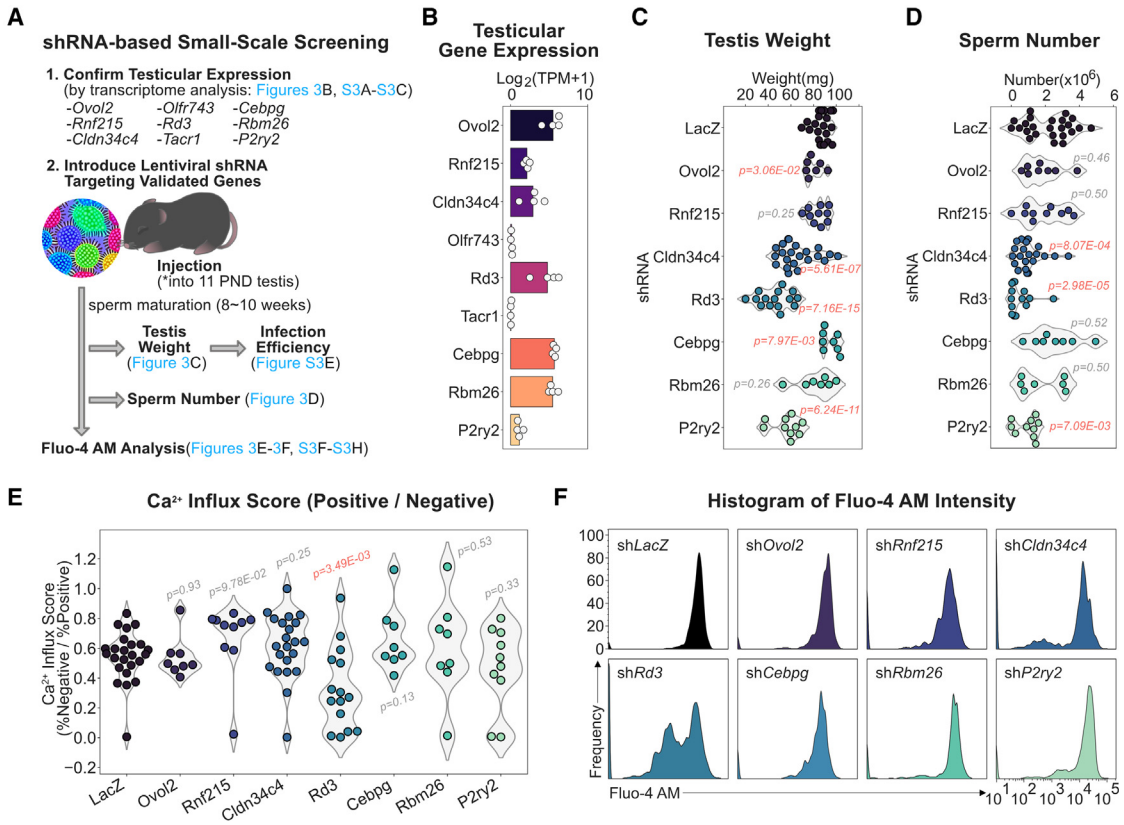

Figure 3. Rd3 is an essential spermatogenesis factor identified through small-scale functional screening

(A) Experimental scheme of shRNA screening.

(B) Transcriptome analysis in testes. Each gene expression shown as $\log_2$(TPM + 1) (see the STAR Methods).

(C) Testicular weight quantification. Data are shown as violin plot according to the following replicates: n = 24 (sh*LacZ*), 7 (sh*Ovol2*), 10 (sh*Rnf215*), 22 (sh*Cldn34c4*), 15 (sh*Rd3*), 8 (sh*Cebpg*), 7 (sh*Rbm26*), and 10 (sh*P2ry2*). p value: unpaired t test. Significant values ($p < 0.05$) are colored orange.

(D) Sperm number quantification. Data are shown as the following replicates: n = 24 (sh*LacZ*), 8 (sh*Ovol2*), 10 (sh*Rnf215*), 22 (sh*Cldn34c4*), 15 (sh*Rd3*), 8 (sh*Cebpg*), 7 (sh*Rbm26*), and 10 (sh*P2ry2*). Statistical evaluation is as described in (C).

(E) Sperm Ca^{2+} influx quantification. Ca^{2+} influx score is as described in Figure S3F. Data are shown as the following replicates: n = 24 (sh*LacZ*), 8 (sh*Ovol2*), 10 (sh*Rnf215*), 22 (sh*Cldn34c4*), 15 (sh*Rd3*), 8 (sh*Cebpg*), 8 (sh*Rbm26*), and 10 (sh*P2ry2*). Statistical evaluation is as described in (C).

(F) Histograms for the representative Fluo-4 AM signal intensity.

cell-type-specific proteomics analysis is typically challenging. Indeed, despite our efforts to identify Rd3 interactors using testicular cells, we encountered significant technical challenges in the process (i.e., low Rd3 expression level per cell, limited number of Rd3-expressing cells, and unavailability of anti-Rd3 antibody for immunoprecipitation). Therefore, we decided to use cells from the retinal cell line Y-79, which express *RD3* endogenously at a high level according to the Cancer Cell Line Encyclopedia dataset,[54] to perform proteomics analysis. Subsequently, gene expression of identified proteins were profiled to narrow down candidates that function in round spermatids.

To this end, using Y-79 cells, *RD3* knockout ($RD3^{-/-}$) cells and those expressing Spot-tagged RD3 (RD3-Spot) were generated. Next, immunoprecipitation was performed using anti-Spot nanobody-conjugated beads (Spot-Trap) on cell lysates prepared from $RD3^{-/-}$ cells and those with RD3-Spot, followed by mass spectrometry. As a result, 269 proteins were found to interact directly or indirectly with RD3 (Figure 5A). In order to search for proteins potentially functioning with RD3 in spermatids, gene expression of these 269 candidates was analyzed using the testicular scRNA-seq data and classified into spermatogenic cell types in Figure 4. Consequently, 49 proteins were found to be highly expressed in round and elongating spermatids (Figures 5B and 5C). GO analysis showed that most of the 49 proteins were related to mitochondria and microtubule function (Figure 5D). To validate Rd3 and mitochondrion interaction in testicular cells, we homogenized testes with Dounce homogenizer and fractionated the homogenates by sequential centrifugation and found that Rd3 was located in the mitochondria fraction (Figure S5A), suggesting that Rd3 interacts with mitochondria in testicular cells.

We next asked how Rd3-mitochondria interaction regulates the function of testicular cells. To gain functional insight into these 49 genes, we developed a signaling pathway analysis tool called Hub-Explorer, which enables the identification of the cell-type-specific signaling pathway based on proteomic and transcriptomic data (Figure 5E; see the STAR Methods). While conventional proteomics studies commonly utilize GO

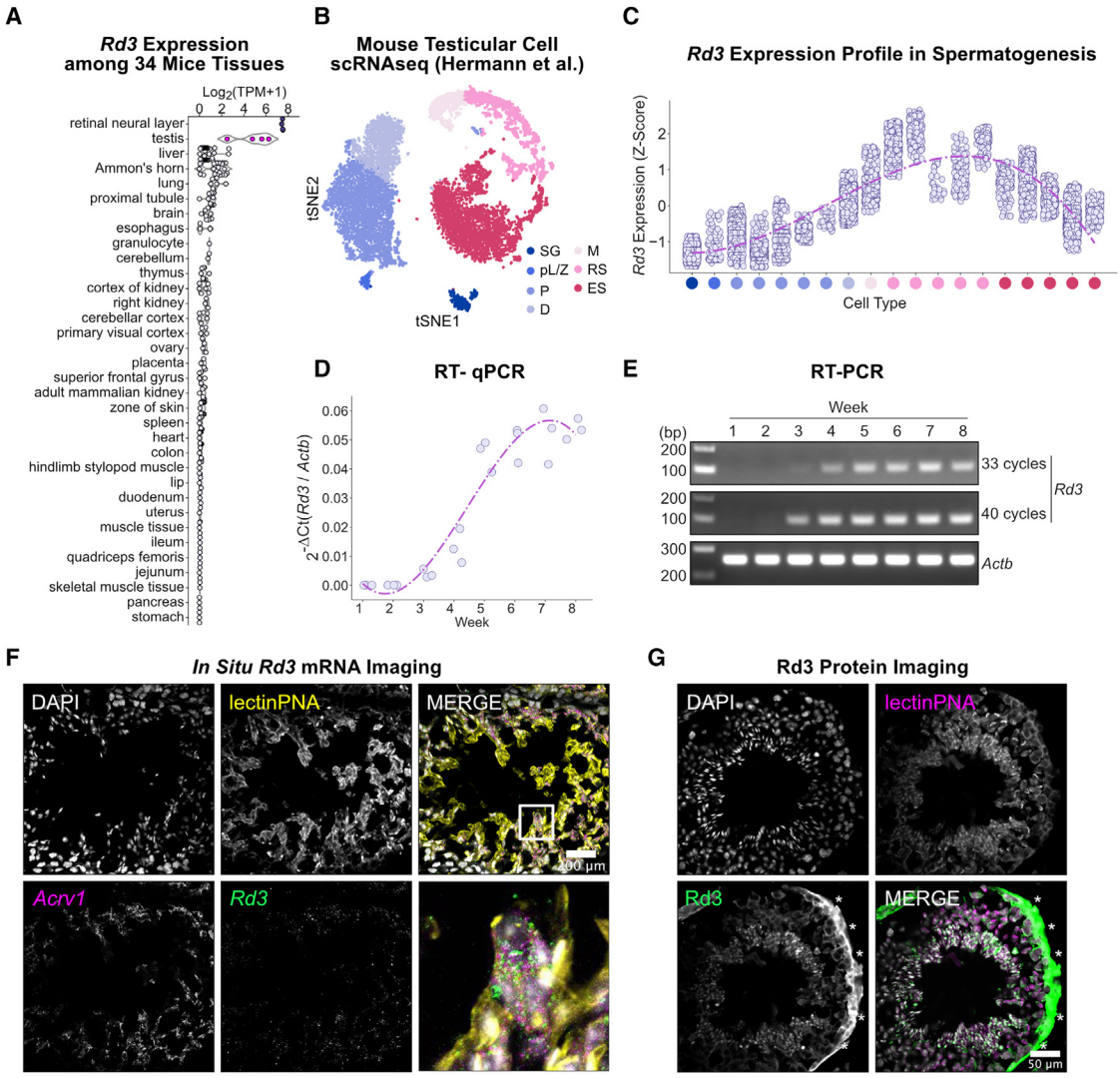

Figure 4. Round spermatid is the specific cell type with high Rd3 expression in testes

(A) Tissue-wide transcriptome analysis of *Rd3*. Adult mice-derived *Rd3* expression is shown as $\log_2$(TPM + 1) values. Testis: magenta; retinal neural layer: midnight blue.

(B) t-Distributed stochastic neighbor embedding (tSNE) plot of mouse testicular cells. Single-cell data (total: 6,693 cells) are clustered as the following cell types: spermatogonium (SG), pre-leptotene/zygotene (pL/Z), pachytene (P), diplotene (D), meiotic cell (M), round spermatid (RS), and elongating spermatid (ES).

(C) *Rd3* expression profiling. x axis: cell types (total: 6,644 cells); y axis: *Rd3* expression shown as *Z* score converted from ln(CPM + 1).

(D and E) *Rd3* expression on different ages. (D) RT-qPCR. (E) RT-PCR.

(F) Hybridization-chain-reaction-based fluorescent *in situ* hybridization (HCR-FISH). Cryo-sectioned testes were probed with *Acrv1* (magenta), *Rd3* (green), DAPI (white), and lectin PNA (yellow), detected by confocal microscope. Scale bar: 200 μm.

(G) Immunohistochemistry of Rd3. Cryo-sectioned adult testes were stained with DAPI (white), lectin PNA (magenta), and Rd3 (green), detected by confocal microscope. Scale bar: 50 μm.

analysis to elucidate the functions of identified proteins, GO analysis alone falls short in revealing the signaling pathways that regulate these identified proteins. To solve this issue, Hub-Explorer was designed to identify the signaling pathway using a GCN according to the following processes.

In the first step, a testicular cell-specific GCN was generated for each of the 49 genes using testicular scRNA-seq expression data. In the second step, gene components in each GCN were applied to GO analysis, and 17 out of 49 genes had the significant GO terms (=hub components: Benjamini-Hochberg false discovery rate < 0.05). In the third step, the Jaccard similarity index was calculated based on the hub components, and these 17 genes were clustered using their calculated index scores through the K-means method (k = 4). Finally, overlapping hub components were extracted as the core signaling pathway from each cluster (Figure 5F). As a result, C1 and C2 clusters, composed of 10 genes, were identified as the major cluster containing the core signaling pathway. These pathways were found

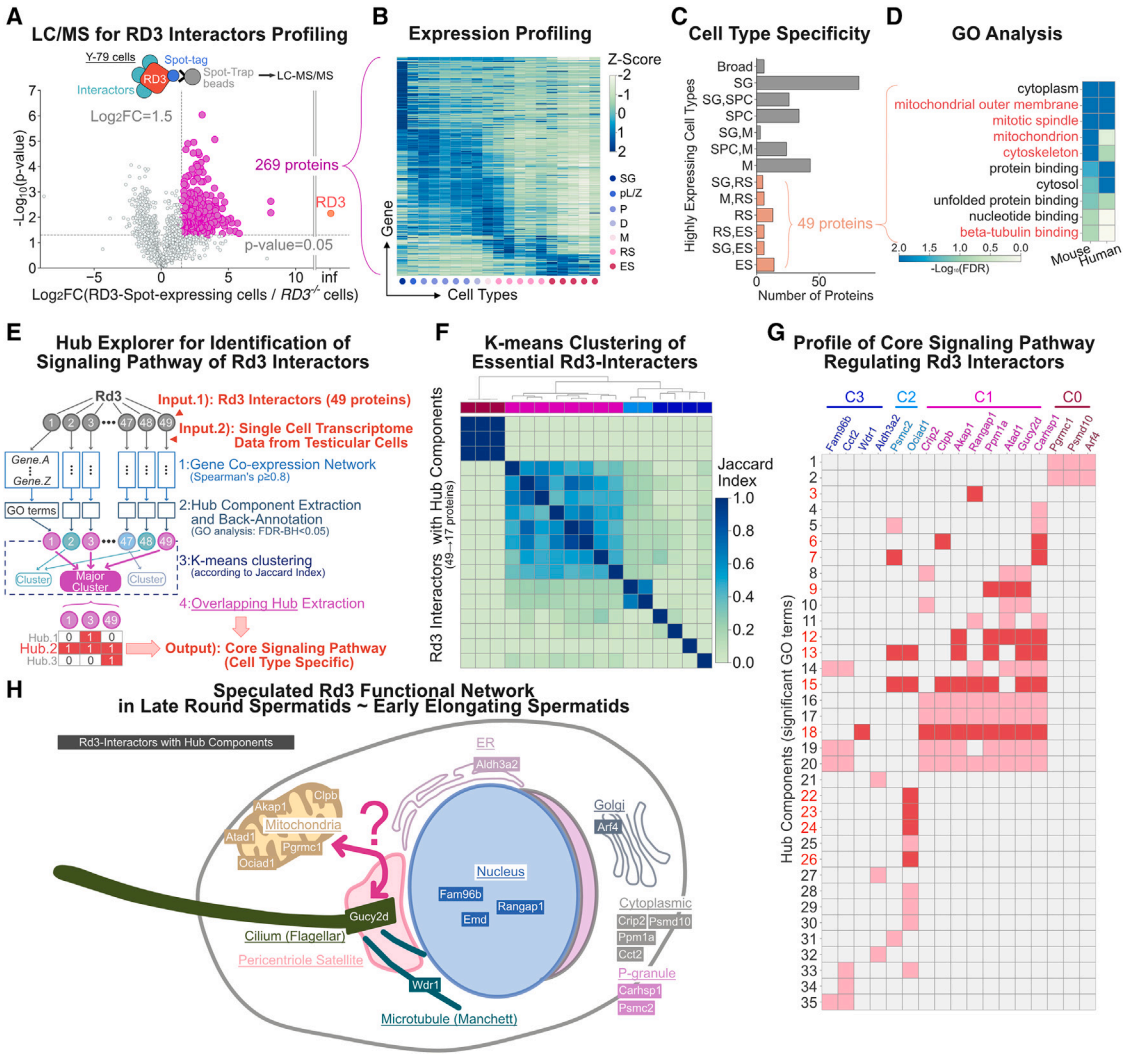

Figure 5. Identification of ciliogenesis-associated Rd3-mitochondria axis by Hub-Explorer analysis

(A) Proteomics for RD3 interactors. Immunoprecipitates obtained by anti-Spot nanobody were analyzed by liquid chromatography-tandem mass spectrometry (LC-MS/MS). Significant proteins (magenta) are shown as $p < 0.05$ and $\log_2$ fold change (RD3-Spot-expressing cells/*RD3*$^{-/-}$ cells) ≧1.5. Experiment was repeated three times (n = 3).

(B) Gene expression profile of 269 significant proteins in testicular cells. 269 proteins gene expression levels shown as *Z* score from testicular gene expression matrix used in Figures 4B, 4C, and S4A. x axis: cell types; y axis: genes. Colored dots indicate the following cell types: SG, pL/Z, P, D, M, RS, and ES.

(C) Cell type classification of 269 proteins on gene expression pattern in testis. Highly expressing cell types were determined by the cell type index (CTI ≧ 0.98; see STAR Methods), shown on the y axis, and the count of proteins in each cell type is shown on the x axis. Orange-colored bars: specific group including spermatid.

(D) Gene Ontology (GO) analysis. 49 proteins analyzed by DAVID software with mouse (left column) and human (right) Ensembl IDs.

(E) Computational process of Hub-Explorer analysis.

(F) Similarity profile of 17 Rd3 interactors with hub components (Benjamini-Hochberg false discovery rate [BH-FDR] < 0.05) according to Jaccard similarity index visualized as a heatmap (both axes: 17 interactors). Each cluster is colored by 4 individual colors (C0: wine red, C1: magenta, C2: deep sky blue, and C3: blue). The annotated hierarchical cluster was used for the benchmark of K-means clustering.

(G) Profile of hub components and core signaling pathways. x axis: 17 candidates clustered and labeled as indicated in (F); y axis: hub components. Core signaling pathway: scarlet; others: Safrano pink. Numbers on the y axis indicate hub components as follows: 1, CatSper complex; 2, sperm head plasma membrane; 3, *centrosome; 4, membrane protein complex; 5, plasma-membrane-bounded cell projection; 6, *sperm midpiece; 7, *9 + 2 motile cilium; 8, non-membrane-bounded organelle; 9, *microtubule cytoskeleton; 10, intracellular non-membrane-bounded organelle; 11, protein-DNA complex; 12, *sperm flagellum; 13, *motile cilium; 14, nuclear-protein-containing complex; 15, *cilium; 16, nucleosome; 17, DNA packaging complex; 18, *cytoskeleton; 19, ribonucleoprotein complex; 20, protein-containing complex; 21, phosphatase complex; 22, *ciliary basal body; 23, *dynein complex; 24, *microtubule; 25, catalytic complex; 26, *axonemal microtubule; 27, protein serine/threonine phosphatase complex; 28, membrane; 29, ubiquitin ligase complex; 30, cytoplasmic microtubule; 31, cell projection; 32, protein phosphatase type 2A complex; 33, cellular anatomical entity; 34, intracellular-protein-containing complex; and 35, spliceosomal complex. *Core signaling pathway (scarlet).

(H) Intracellular localization of 17 candidate interactors with hub components in late round spermatids and early elongating spermatids.

to be associated with ciliogenesis, which contributes to sperm flagellar development (Figure 5G), suggesting that either the Rd3-mitochondria interaction regulates ciliogenesis or ciliogenesis regulates the Rd3-mitochondria interaction (Figures 5H and S5B). Additional analysis using *Rd3*-correlated genes in the testis also supported this conclusion: Rd3 is associated with ciliogenesis (Figures S5C–S5E). Although conventional GO analysis was unable to identify the ciliogenesis-related GO terms (Figure 5D), this was successfully achieved by Hub-Explorer.

Rd3 modulates mitochondrial spatial distribution under ciliogenesis-induction-derived oxidative stress

Based on the proteomics and Hub-Explorer analyses in Figures 5D and 5G, we hypothesized that the Rd3-mitochondria interaction regulates ciliogenesis or that ciliogenesis regulates the Rd3-mitochondria interaction. To examine this hypothesis, we tried to induce ciliogenesis in Y-79 cells, but induction efficiency was low. Therefore, we examined other cell lines and decided to use SH-SY5Y cells, which express *RD3* endogenously[54] and have ciliogenesis capability.[55,56] Prior to ciliogenesis analysis, we first examined whether the RD3-mitochondria interaction occurs in SH-SY5Y cells. Using immunocytochemistry analysis, we demonstrated that RD3 co-localized with the mitochondria marker Tomm20 (Figure 6A), suggesting that RD3 also interacts with mitochondria in SH-SY5Y cells. Next, we tried to clarify the relationship between the RD3-mitochondria interaction and ciliogenesis. To this end, we induced ciliogenesis by serum starvation and investigated the frequency of cilia formation and cilium length between *RD3*$^{-/-}$ cells and those expressing exogenous RD3 (Figures 6B–6D and S6A). Despite a thorough investigation, no difference was observed, suggesting that the Rd3-mitochondria interaction does not regulate ciliogenesis (Figure 6E). Based on these results and because RD3 was also found to associate with tubulin in the proteomics study (Figure 5D), we hypothesized that ciliogenesis affects RD3-mitochondria dynamics. To examine this, we quantified mitochondrial distribution under the induction of ciliogenesis (Figure S6B). From the result, mitochondria were found to be dispersed under the induction of ciliogenesis compared to the resting state. However, in *RD3*$^{-/-}$ cells, mitochondria dispersion was not observed (Figures 6F–6H, S6C, and S6D). Previous studies have suggested that the induction of ciliogenesis is associated with accumulation of reactive oxygen species (ROS).[57,58] Other studies have further shown that ROS accumulation is modulated by mitochondrial dispersion.[59–61] Based on these findings, we hypothesized that RD3-regulated mitochondria dispersion reduces excessive ROS accumulation, promoted by ciliogenesis induction. To examine this hypothesis, we quantified the mitochondrial ROS level under ciliogenesis induction by the H_2O_2 probe MitoPY1 and found that ROS is more accumulated in *RD3*$^{-/-}$ cells (Figure 6I), suggesting that RD3-regulated mitochondrial dispersion decreases oxidative stress under ciliogenesis. Taken together, RD3 interacts with mitochondria, regulates mitochondria dispersion, and reduces the amount of ROS accumulation promoted by the induction of ciliogenesis (Figure 6J).

We next questioned whether these cell line results were relevant to testicular cells. Figure 3 indicates that sh*Rd3* introduction in the testes reduced cell numbers. With the observed increase in ROS accumulation in *Rd3*$^{-/-}$ cells (Figure 6I), it is plausible to hypothesize that sh*Rd3* might elevate ROS levels, leading to cell death. To assess the impact of sh*Rd3* on round spermatid viability, we introduced sh*Rd3* into testes and found that *Rd3* knockdown significantly reduces the viability of Bsg^{+} testicular cells at 8 weeks more than at 5 weeks, suggesting a pronounced effect of *Rd3* knockdown on later-stage spermatogenic cells, including round spermatids (Figure S7). To explore the relationship between this effect and ROS levels, we administered N-acetyl-cysteine (NAC), an antioxidant, and successfully mitigated the phenotype (Figure S8). These results endorse the role of Rd3 in modulating ROS accumulation during spermatogenesis, which was also corroborated by findings in Figures 3 and 6J.

DISCUSSION

In vivo genome-wide screening approach using testicular cells

CRISPR-Cas9 sgRNA library screening is extensively utilized both *in vitro* and *in vivo* to elucidate the molecular mechanisms of biological phenomena based on cellular growth. Despite its widespread application, performing screening on biochemical activities, not directly related to growth, is challenging. Addressing this limitation, we recently established the revival screening method by leveraging repeated sorting and realized biochemical-activity-targeted screening in cell lines. Building on this achievement, this study adapted revival screening to establish a screening system targeting biochemical activity in mice testes, thereby providing proof of concept for *in vivo* screening.

For successful implementation of *in vivo* genome-wide screening, we considered that the efficiency of sgRNA introduction is a major issue to be addressed. Our research has demonstrated that the efficiency of sgRNA introduction is influenced by a variety of factors, including the method of sgRNA delivery, viral tropism, and the duration of sgRNA expression in the targeted tissues. In this study, we achieved substantial sgRNA coverage in male germ cells by employing a novel technique that combines injection through seminiferous tubules and the use of pseudotyped lentiviruses (pLVs), especially SVF proteins. It is important to note that the choice of pLVs significantly affects sgRNA induction efficiency, underscoring the importance of selecting pLVs with an appropriate engineering history.

However, our attempts to maintain long-term sgRNA expression in male germ cells were not entirely successful. We observed a decrease in the sgRNA-derived indel population over time. This decrease occurred despite sustained infectivity of the lentivirus, as evidenced by persistent expression of a fluorescent protein marker (Figure S9). We hypothesize that the observed decrease in the sgRNA population might be attributed to activation of a DNA damage response, specifically through the ATM-γH2AX axis. This response is typically limited to the nuclei of leptotene and zygotene stages of germ cell development.[62–65] The induced DNA double-strand breaks by Cas9 are likely to be a trigger for this response, leading to the reduction in sgRNA population. In the future, it may be beneficial to explore alternative techniques, such as CRISPR interference/activation (CRISPRi/a)[66,67] and CRISPR-Cas13,[68,69] to enhance screening

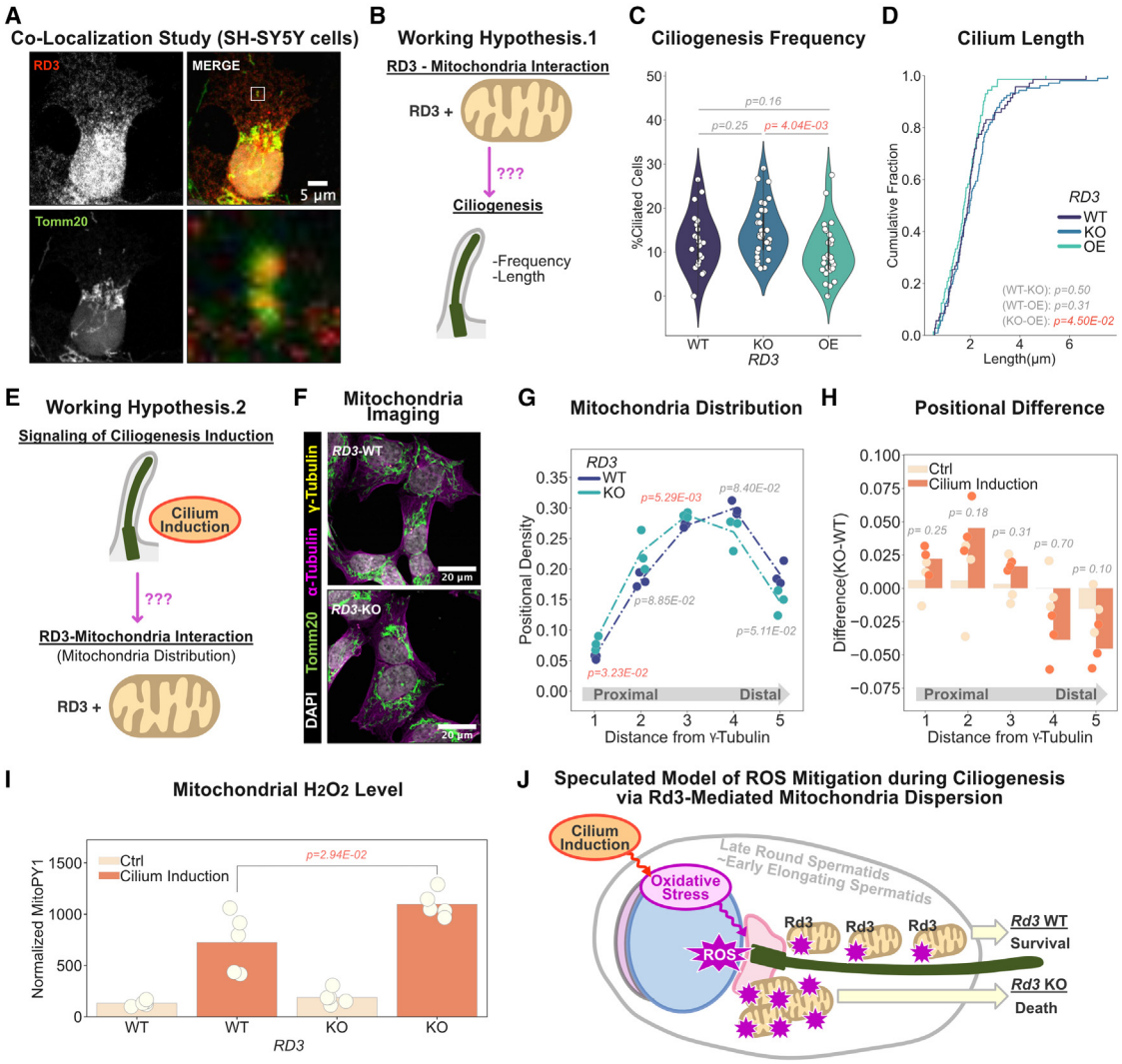

Figure 6. RD3 modulates mitochondrial spatial distribution under ciliogenesis-induction-derived oxidative stress

(A) RD3 and mitochondria co-localization study. SPOT-tagged RD3 SH-SY5Y cells stained with anti-RD3 (red) and Alexa 488-conjugated Tomm20 (green) antibodies with DAPI (white) and imaged by confocal microscope. Scale bar: 5 μm. Cell: SH-SY5Y.

(B and E) Working hypothesis.

(C) Quantification of ciliogenesis frequency. Primary cilium frequency quantified using filtered sections (30–50 cells per section). *RD3*-wild type (WT): 803 cells (navy); KO: 1,269 cells (cobalt blue); and overexpression (OE): 1,141 cells (light green) are shown as a violin plot. Each frequency per section is shown as white dots. p value: an unpaired t test. $p < 0.05$: orange. Experiments were repeated three times (n = 3).

(D) Cilium length quantification. Primary cilium length quantified by Nikon NIS-Element software using filtered sections. *RD3*-WT: 71 cilia (navy); KO: 106 cilia (cobalt blue); and OE: 72 cilia (light green) are shown as a cumulative plot. Statistical analysis was conducted as described in (C).

(F) Mitochondria distribution imaging. Ciliogenesis was induced by serum starvation. Cells were stained with anti-α-tubulin (magenta), Alexa 488-conjugated Tomm20 (green), and Alexa 647-conjugated γ-tubulin (yellow) antibodies and DAPI (white), imaged by confocal microscope. Scale bar: 20 μm.

(G) Mitochondrial distribution quantification. The mitochondria distribution index calculated at 5 different spots is defined by the distance from the γ-tubulin signal. Quantification was performed by around 30 cells per replicate. Quantifications were conducted three times (n = 3). p value: an unpaired t test. $p < 0.05$: orange.

(H) Mitochondrial distribution differences. Distribution difference between *RD3*-WT and KO is shown as barplot. p value: an unpaired t test.

(I) Mitochondrial H_2O_2 evaluation. MitoPY1 and Hoechst33342 signals measured by plate reader. Raw MitoPY1 signal was normalized by Hoechst33342, multiplied by 1×10^4, and shown as a bar plot. p value: an unpaired t test. $p < 0.05$: orange. Experiments were repeated five times (n = 5).

(J) Summary of Rd3-mitochondria spatial dynamics under cilium-induction-oriented oxidative stress.

efficiency in specific cell types. These alternatives could circumvent the challenges encountered with genome editing in certain cellular contexts.

Rd3 molecular function during spermatogenesis

In our study, Rd3 emerged as a critical factor influencing spermatogenesis, as demonstrated by the results presented in

Figures 3 and 4. While existing research predominantly recognizes Rd3 as an inhibitor of retinal guanylyl cyclase (RetGC1/2), primarily influencing cGMP production in retinogenesis,[25,26,46] its role in spermatogenesis has yet to be investigated. Hub-Explorer analysis suggests that the interaction between Rd3 and mitochondria modulates mitochondria's localization in the context of ciliogenesis. This interaction reduces ROS accumulation by promoting mitochondrial dispersion from the tubulin organizing center. Although cilium structures are different between rod/cone cells and round spermatids, ciliogenesis is a common cell state in both cell types during development, suggesting a functional overlap of Rd3 across these processes. *In vivo* rescue experiments using NAC indicated a modulatory role of Rd3 in ROS management in testicular cells (Figure S8). However, the incomplete restoration observed suggests additional, unexplored mechanisms at play. Future research should focus on elucidating these interactions, in particular examining mitochondrial localization and cGMP production in round spermatids to determine if Rd3's role is cell-type specific.

Limitations

This study has successfully established proof of concept for a testes-targeted *in vivo* screening system. Nonetheless, it is essential to address several limitations inherent in this system. First, a notable limitation concerns the impact of CRISPR-Cas9 editing on male germ cells. Specifically, our observations, detailed in the discussion, indicate a reduction in the Rosa26 knockout cell population despite ongoing infection. This phenomenon resulted in a constrained pool of feasible candidate sgRNAs and genes. Indeed, known Ca^{2+} channels were not identified in this screening. To mitigate this limitation, employing an alternative methodology, such as the use of a pooled library tailored for various cell types (including CRISPRi, CRISPRa, or CRISPR-Cas13 systems), might be beneficial.

The second major challenge involves the technical difficulty in specifically targeting type A spermatogonia for sgRNA introduction. Although SVF-pLVs effectively enhanced sgRNA delivery to type A spermatogonia, unintentional delivery to other germ cells or Sertoli cells was also noted. In our approach, we treated Cas9 mice with busulfan to deplete most germ cells except spermatogonia prior to viral introduction. However, discrepancies in infection efficiency were evident (Figure S10). Future advancements in developing lentiviral vectors specific to certain cell types are critical for more precise investigation into cell-type-specific biology and mechanisms.

In addition, our Hub-Explorer tool encounters a technical limitation due to its reliance on the type of expression data matrix utilized. Within the testicular environment, scRNA-seq data enable the capture of a spectrum of cell types in various developmental stages, allowing for the creation of an accurate GCN that mirrors expression dynamics. In contrast, the analysis of adult retinal scRNA-seq data, characterized by fully differentiated and distinct cell types, presents challenges in delineating time-scaled sequential gene expression dynamics. Therefore, the selection of appropriate datasets is vital for the effective utilization of this analytical instrument.

STAR★METHODS

Detailed methods are provided in the online version of this paper and include the following:

- KEY RESOURCES TABLE
- RESOURCE AVAILABILITY
  - Lead contact
  - Materials availability
  - Data and code availability
- EXPERIMENTAL MODEL AND SUBJECT DETAILS
  - Animals
  - Cell lines
- METHOD DETAILS
  - Lentivirus production
  - Titer evaluation for the lentivirus encoding fluorescent protein
  - Titer evaluation for the lentivirus encoding puromycin-resistant protein
  - Determination of mice age for virus injection
  - Capacitation medium
  - Sperm capacitation and flow cytometry analysis
  - Immunohistochemistry (IHC)
  - Testis dissociation
  - *In vivo* knockout study by indel analysis
  - *In vivo* knockout study by Gcna1 knockout analysis
  - Infection efficiency investigation by flow cytometry
  - Scanning electron microscope (SEM)
  - Sperm *in vivo* genome-wide screening
  - sgRNA coverage analysis
  - Reverse transcription (RT)-PCR and quantitative RT-PCR (RT-qPCR)
  - shRNA-based small-scaled screening
- QUANTIFICATION AND STATISTICAL ANALYSIS
  - Quantification and statistical analysis for experimental data
  - Tissue-wide comparative study for characterizing gene expression
  - *Rd3* expression profiling in testicular cells and retinal cells
  - Analysis for *in vivo* genome-wide screening
  - Analysis for library coverage investigation
  - Hub-Explorer
  - Mass spectrometry analysis for profiling RD3 interactors
  - Gene ontology (GO) analysis
  - Mitochondrial distribution analysis
  - Ciliogenesis evaluation

SUPPLEMENTAL INFORMATION

Supplemental information can be found online at https://doi.org/10.1016/j.xgen.2024.100510.

ACKNOWLEDGMENTS

We thank Takuya Yamamoto, Kyoto University, for discussion of Hub-Explorer; Tomonori Nakamura and Yukiko Ishikura, Kyoto University, for advice on germ cell experimentation; So Nagaoka, Nara Medical University,

for discussion of plasmid design; Kouichi Hasegawa, CUORiPS Inc., for the technical discussion of virus injection methods; Yasutaka Okabe, Osaka University, for advice on the testis dissociation protocol; and the Division of Electron Microscopic Study, Center for Anatomical Studies, Graduate School of Medicine, Kyoto University, for SEM imaging and discussion. We thank members of the Suzuki lab for discussions, especially Wen Ann Wee for English editing. This work was supported by Grants-in-Aid for Scientific Research on Innovative Areas (grant no. 21H00230 to J.S.), the Japan Science and Technology Agency (JST) Fusion Oriented Research for Disruptive Science and Technology (FOREST) (grant no. JPMJFR2162 to J.S.), the Joint Usage and Joint Research Programs of the Institute of Advanced Medical Sciences of Tokushima University (to J.S.), a Grant-in-Aid for Research Activity Start-up (grant no. 22K20972 to Y.N.), JST SPRING (grant no. JPMJSP2110 to Y.N.), and The Sasakawa Scientific Research Grant from the Japan Science Society (grant no. 2022-4005 to Y.N.).

AUTHOR CONTRIBUTIONS

Y.N. and J.S. designed the overall research and interpreted experimental results. Y.N. conducted most experiments, including *in vivo* genome-wide screening establishment, computational analysis, and *in vivo*/*in vitro* molecular biology experiments. Y.O. performed the quantification study of mitochondrial distribution. T.M. designed the primary cilium experiment. M.M. realized the concept of the repeated sorting-based sgRNA enrichment method, called revival screening. H.K. performed the mass spectrometry analysis. Y.N. and J.S. wrote the manuscript.

DECLARATION OF INTERESTS

J.S. and Y.N. are inventors on a patent application of the *in vivo* genome-wide screening method toward spermatogenesis.

DECLARATION OF GENERATIVE AI AND AI-ASSISTED TECHNOLOGIES IN THE WRITING PROCESS

During the preparation of this work, the authors used Grammarly and ChatGPT4 for English language editing after completing the initial writing by the authors. After using these tools, the authors reviewed and edited the content as needed and take full responsibility for the content of the publication.

Received: June 21, 2023
Revised: December 10, 2023
Accepted: February 6, 2024
Published: March 5, 2024

REFERENCES

1. Mani, R., St.Onge, R.P., Hartman, J.L., Giaever, G., and Roth, F.P. (2008). Defining genetic interaction. Proc. Natl. Acad. Sci. USA *105*, 3461–3466. https://doi.org/10.1073/pnas.0712255105.
2. Gupta, G.D., Coyaud, É., Gonçalves, J., Mojarad, B.A., Liu, Y., Wu, Q., Gheiratmand, L., Comartin, D., Tkach, J.M., Cheung, S.W.T., et al. (2015). A Dynamic Protein Interaction Landscape of the Human Centrosome-Cilium Interface. Cell *163*, 1484–1499. https://doi.org/10.1016/j.cell.2015.10.065.
3. Costanzo, M., VanderSluis, B., Koch, E.N., Baryshnikova, A., Pons, C., Tan, G., Wang, W., Usaj, M., Hanchard, J., Lee, S.D., et al. (2016). A global genetic interaction network maps a wiring diagram of cellular function. Science *353*, aaf1420. https://doi.org/10.1126/science.aaf1420.
4. Smith, V., Botstein, D., and Brown, P.O. (1995). Genetic footprinting: a genomic strategy for determining a gene's function given its sequence. Proc. Natl. Acad. Sci. USA *92*, 6479–6483. https://doi.org/10.1073/pnas.92.14.6479.
5. Jansen, G., Hazendonk, E., Thijssen, K.L., and Plasterk, R.H.A. (1997). Reverse genetics by chemical mutagenesis in Caenorhabditis elegans. Nat. Genet. *17*, 119–121. https://doi.org/10.1038/ng0997-119.
6. Fire, A., Xu, S., Montgomery, M.K., Kostas, S.A., Driver, S.E., and Mello, C.C. (1998). Potent and specific genetic interference by double-stranded RNA in Caenorhabditis elegans. Nature *391*, 806–811. https://doi.org/10.1038/35888.
7. Winzeler, E.A., Shoemaker, D.D., Astromoff, A., Liang, H., Anderson, K., Andre, B., Bangham, R., Benito, R., Boeke, J.D., Bussey, H., et al. (1999). Functional Characterization of the S. cerevisiae Genome by Gene Deletion and Parallel Analysis. Science *285*, 901–906. https://doi.org/10.1126/science.285.5429.901.
8. Tsien, J.Z., Chen, D.F., Gerber, D., Tom, C., Mercer, E.H., Anderson, D.J., Mayford, M., Kandel, E.R., and Tonegawa, S. (1996). Subregion- and Cell Type–Restricted Gene Knockout in Mouse Brain. Cell *87*, 1317–1326. https://doi.org/10.1016/S0092-8674(00)81826-7.
9. Skarnes, W.C., Rosen, B., West, A.P., Koutsourakis, M., Bushell, W., Iyer, V., Mujica, A.O., Thomas, M., Harrow, J., Cox, T., et al. (2011). A conditional knockout resource for the genome-wide study of mouse gene function. Nature *474*, 337–342. https://doi.org/10.1038/nature10163.
10. Kuhn, M., Santinha, A.J., and Platt, R.J. (2021). Moving from in vitro to in vivo CRISPR screens. Gene and Genome Editing *2*, 100008. https://doi.org/10.1016/j.ggedit.2021.100008.
11. VanDusen, N.J., Lee, J.Y., Gu, W., Butler, C.E., Sethi, I., Zheng, Y., King, J.S., Zhou, P., Suo, S., Guo, Y., et al. (2021). Massively parallel in vivo CRISPR screening identifies RNF20/40 as epigenetic regulators of cardiomyocyte maturation. Nat. Commun. *12*, 4442. https://doi.org/10.1038/s41467-021-24743-z.
12. Ruetz, T.J., Kashiwagi, C.M., Morton, B., Yeo, R.W., Leeman, D.S., Morgens, D.W., Tsui, C.K., Li, A., Bassik, M.C., and Brunet, A. (2021). In vitro and in vivo CRISPR-Cas9 screens reveal drivers of aging in neural stem cells of the brain. Preprint at bioRxiv. https://doi.org/10.1101/2021.11.23.469762.
13. Wertz, M.H., Mitchem, M.R., Pineda, S.S., Hachigian, L.J., Lee, H., Lau, V., Powers, A., Kulicke, R., Madan, G.K., Colic, M., et al. (2020). Genome-wide In Vivo CNS Screening Identifies Genes that Modify CNS Neuronal Survival and mHTT Toxicity. Neuron *106*, 76–89. https://doi.org/10.1016/j.neuron.2020.01.004.
14. Keys, H.R., and Knouse, K.A. (2022). Genome-scale CRISPR screening in a single mouse liver. Cell Genomics *2*, 100217. https://doi.org/10.1016/j.xgen.2022.100217.
15. Jia, Y., Li, L., Lin, Y.H., Gopal, P., Shen, S., Zhou, K., Yu, X., Sharma, T., Zhang, Y., Siegwart, D.J., et al. (2022). In vivo CRISPR screening identifies BAZ2 chromatin remodelers as druggable regulators of mammalian liver regeneration. Cell Stem Cell *29*, 372–385.e8. https://doi.org/10.1016/j.stem.2022.01.001.
16. Maruoka, M., Zhang, P., Mori, H., Imanishi, E., Packwood, D.M., Harada, H., Kosako, H., and Suzuki, J. (2021). Caspase cleavage releases a nuclear protein fragment that stimulates phospholipid scrambling at the plasma membrane. Mol. Cell *81*, 1397–1410.e9. https://doi.org/10.1016/j.molcel.2021.02.025.
17. Austin, C. (1951). Observations on the Penetration of the Sperm into the Mammalian Egg. Aust. Jnl. Of Bio. Sci. *4*, 581. https://doi.org/10.1071/BI9510581.
18. Chang, M.C. (1951). Fertilizing Capacity of Spermatozoa deposited into the Fallopian Tubes. Nature *168*, 697–698. https://doi.org/10.1038/168697b0.
19. Austin, C.R. (1952). The 'Capacitation' of the Mammalian Sperm. Nature *170*, 326. https://doi.org/10.1038/170326a0.
20. Loeb, J. (1915). On the Nature of the Conditions Which Determine or Prevent the Entrance of the Spermatozoon Into the Egg. Am. Nat. *49*, 257–285. https://doi.org/10.1086/279480.
21. Visconti, P.E., Galantino-Homer, H., Moore, G.D., Bailey, J.L., Ning, X., Fornes, M., and Kopf, G.S. (1998). The Molecular Basis of Sperm Capacitation. J. Androl. *19*, 242–248. https://doi.org/10.1002/j.1939-4640.1998.tb01994.x.

22. Suarez, S.S. (2008). Control of hyperactivation in sperm. Hum. Reprod. Update *14*, 647–657. https://doi.org/10.1093/humupd/dmn029.

23. Xia, J., and Ren, D. (2009). The BSA-induced Ca(2+) influx during sperm capacitation is CATSPER channel-dependent. Reprod. Biol. Endocrinol. *7*, 119. https://doi.org/10.1186/1477-7827-7-119.

24. Friedman, J.S., Chang, B., Kannabiran, C., Chakarova, C., Singh, H.P., Jalali, S., Hawes, N.L., Branham, K., Othman, M., Filippova, E., et al. (2006). Premature truncation of a novel protein, RD3, exhibiting subnuclear localization is associated with retinal degeneration. Am. J. Hum. Genet. *79*, 1059–1070. https://doi.org/10.1086/510021.

25. Azadi, S., Molday, L.L., and Molday, R.S. (2010). RD3, the protein associated with Leber congenital amaurosis type 12, is required for guanylate cyclase trafficking in photoreceptor cells. Proc. Natl. Acad. Sci. USA *107*, 21158–21163. https://doi.org/10.1073/pnas.1010460107.

26. Peshenko, I.V., Olshevskaya, E.V., Azadi, S., Molday, L.L., Molday, R.S., and Dizhoor, A.M. (2011). Retinal Degeneration 3 (RD3) Protein Inhibits Catalytic Activity of Retinal Membrane Guanylyl Cyclase (RetGC) and Its Stimulation by Activating Proteins. Biochemistry *50*, 9511–9519. https://doi.org/10.1021/bi201342b.

27. Watanabe, S., Kanatsu-Shinohara, M., and Shinohara, T. (2019). Sendai virus-mediated transduction of mammalian spermatogonial stem cells. Biol. Reprod. *100*, 523–534. https://doi.org/10.1093/biolre/ioy192.

28. Shinohara, T., and Kanatsu-Shinohara, M. (2020). Transgenesis and Genome Editing of Mouse Spermatogonial Stem Cells by Lentivirus Pseudotyped with Sendai Virus F Protein. Stem Cell Rep. *14*, 447–461. https://doi.org/10.1016/j.stemcr.2020.02.001.

29. Picher, Á.J., Budeus, B., Wafzig, O., Krüger, C., García-Gómez, S., Martínez-Jiménez, M.I., Díaz-Talavera, A., Weber, D., Blanco, L., and Schneider, A. (2016). TruePrime is a novel method for whole-genome amplification from single cells based on TthPrimPol. Nat. Commun. *7*, 13296. https://doi.org/10.1038/ncomms13296.

30. Kanatsu-Shinohara, M., Toyokuni, S., and Shinohara, T. (2004). Transgenic Mice Produced by Retroviral Transduction of Male Germ Line Stem Cells In Vivo1. Biol. Reprod. *71*, 1202–1207. https://doi.org/10.1095/biolreprod.104.031294.

31. Ikawa, M., Tergaonkar, V., Ogura, A., Ogonuki, N., Inoue, K., and Verma, I.M. (2002). Restoration of spermatogenesis by lentiviral gene transfer: Offspring from infertile mice. Proc. Natl. Acad. Sci. USA *99*, 7524–7529. https://doi.org/10.1073/pnas.072207299.

32. Wang, F., Zhang, Q., Cao, J., Huang, Q., and Zhu, X. (2008). The microtubule plus end-binding protein EB1 is involved in Sertoli cell plasticity in testicular seminiferous tubules. Exp. Cell Res. *314*, 213–226. https://doi.org/10.1016/j.yexcr.2007.09.022.

33. Kinoh, H., Inoue, M., Washizawa, K., Yamamoto, T., Fujikawa, S., Tokusumi, Y., Iida, A., Nagai, Y., and Hasegawa, M. (2004). Generation of a recombinant Sendai virus that is selectively activated and lyses human tumor cells expressing matrix metalloproteinases. Gene Ther. *11*, 1137–1145. https://doi.org/10.1038/sj.gt.3302272.

34. Enders, G.C., and May, J.J. (1994). Developmentally Regulated Expression of a Mouse Germ Cell Nuclear Antigen Examined from Embryonic Day 11 to Adult in Male and Female Mice. Dev. Biol. *163*, 331–340. https://doi.org/10.1006/dbio.1994.1152.

35. Tokuda, M., Kadokawa, Y., Kurahashi, H., and Marunouchi, T. (2007). CDH1 Is a Specific Marker for Undifferentiated Spermatogonia in Mouse Testes. Biol. Reprod. *76*, 130–141. https://doi.org/10.1095/biolreprod.106.053181.

36. Chen, H., Fok, K.L., Yu, S., Jiang, J., Chen, Z., Gui, Y., Cai, Z., and Chan, H.C. (2011). CD147 is required for matrix metalloproteinases-2 production and germ cell migration during spermatogenesis. Mol. Hum. Reprod. *17*, 405–414. https://doi.org/10.1093/molehr/gar013.

37. Buaas, F.W., Kirsh, A.L., Sharma, M., McLean, D.J., Morris, J.L., Griswold, M.D., de Rooij, D.G., and Braun, R.E. (2004). Plzf is required in adult male germ cells for stem cell self-renewal. Nat. Genet. *36*, 647–652. https://doi.org/10.1038/ng1366.

38. Hobbs, R.M., Fagoonee, S., Papa, A., Webster, K., Altruda, F., Nishinakamura, R., Chai, L., and Pandolfi, P.P. (2012). Functional Antagonism between Sall4 and Plzf Defines Germline Progenitors. Cell Stem Cell *10*, 284–298. https://doi.org/10.1016/j.stem.2012.02.004.

39. Vara, C., Paytuví-Gallart, A., Cuartero, Y., le Dily, F., García, F., Salvà-Castro, J., Gómez-H, L., Julià, E., Moutinho, C., Aiese Cigliano, R., et al. (2019). Three-Dimensional Genomic Structure and Cohesin Occupancy Correlate with Transcriptional Activity during Spermatogenesis. Cell Rep. *28*, 352–367.e9. https://doi.org/10.1016/j.celrep.2019.06.037.

40. Du Plessis, S.S., Cabler, S., McAlister, D.A., Sabanegh, E., and Agarwal, A. (2010). The effect of obesity on sperm disorders and male infertility. Nat. Rev. Urol. *7*, 153–161. https://doi.org/10.1038/nrurol.2010.6.

41. Palmer, N.O., Bakos, H.W., Fullston, T., and Lane, M. (2012). Impact of obesity on male fertility, sperm function and molecular composition. Spermatogenesis *2*, 253–263. https://doi.org/10.4161/spmg.21362.

42. Jin, S.K., and Yang, W.X. (2016). Factors and pathways involved in capacitation: how are they regulated? Oncotarget *8*, 3600–3627. https://doi.org/10.18632/oncotarget.12274.

43. Fujihara, Y., Murakami, M., Inoue, N., Satouh, Y., Kaseda, K., Ikawa, M., and Okabe, M. (2010). Sperm equatorial segment protein 1, SPESP1, is required for fully fertile sperm in mouse. J. Cell Sci. *123*, 1531–1536. https://doi.org/10.1242/jcs.067363.

44. Sanjana, N.E., Shalem, O., and Zhang, F. (2014). Improved vectors and genome-wide libraries for CRISPR screening. Nat. Methods *11*, 783–784. https://doi.org/10.1038/nmeth.3047.

45. Bastian, F.B., Roux, J., Niknejad, A., Comte, A., Fonseca Costa, S.S., de Farias, T.M., Moretti, S., Parmentier, G., de Laval, V.R., Rosikiewicz, M., et al. (2021). The Bgee suite: integrated curated expression atlas and comparative transcriptomics in animals. Nucleic Acids Res. *49*, D831–D847. https://doi.org/10.1093/nar/gkaa793.

46. Molday, L.L., Jefferies, T., and Molday, R.S. (2014). Insights into the role of RD3 in guanylate cyclase trafficking, photoreceptor degeneration, and Leber congenital amaurosis. Front. Mol. Neurosci. *7*.

47. Aravindan, S., Somasundaram, D.B., Kam, K.L., Subramanian, K., Yu, Z., Herman, T.S., Fung, K.M., and Aravindan, N. (2017). Retinal Degeneration Protein 3 (RD3) in normal human tissues: Novel insights. Sci. Rep. *7*, 13154. https://doi.org/10.1038/s41598-017-13337-9.

48. Hermann, B.P., Cheng, K., Singh, A., Roa-De La Cruz, L., Mutoji, K.N., Chen, I.C., Gildersleeve, H., Lehle, J.D., Mayo, M., Westernströer, B., et al. (2018). The Mammalian Spermatogenesis Single-Cell Transcriptome, from Spermatogonial Stem Cells to Spermatids. Cell Rep. *25*, 1650–1667. https://doi.org/10.1016/j.celrep.2018.10.026.

49. Reddi, P.P., Flickinger, C.J., and Herr, J.C. (1999). Round Spermatid-Specific Transcription of the Mouse SP-10 Gene Is Mediated by a 294-Base Pair Proximal Promoter1. Biol. Reprod. *61*, 1256–1266. https://doi.org/10.1095/biolreprod61.5.1256.

50. Fujihara, Y., Herberg, S., Blaha, A., Panser, K., Kobayashi, K., Larasati, T., Novatchkova, M., Theussl, H.C., Olszanska, O., Ikawa, M., et al. (2021). The conserved fertility factor SPACA4/Bouncer has divergent modes of action in vertebrate fertilization. Proc. Natl. Acad. Sci. USA *118*, e2108777118. https://doi.org/10.1073/pnas.2108777118.

51. Van Hove, I., De Groef, L., Boeckx, B., Modave, E., Hu, T.T., Beets, K., Etienne, I., Van Bergen, T., Lambrechts, D., Moons, L., et al. (2020). Single-cell transcriptome analysis of the Akimba mouse retina reveals cell-type-specific insights into the pathobiology of diabetic retinopathy. Diabetologia *63*, 2235–2248. https://doi.org/10.1007/s00125-020-05218-0.

52. Grant, G.R., Farkas, M.H., Pizarro, A.D., Lahens, N.F., Schug, J., Brunk, B.P., Stoeckert, C.J., Hogenesch, J.B., and Pierce, E.A. (2011). Comparative analysis of RNA-Seq alignment algorithms and the RNA-Seq unified mapper (RUM). Bioinformatics *27*, 2518–2528. https://doi.org/10.1093/bioinformatics/btr427.

53. Lee, M.C., and Damjanov, I. (1984). Anatomic distribution of lectin-binding sites in mouse testis and epididymis. Differentiation *27*, 74–81. https://doi.org/10.1111/j.1432-0436.1984.tb01410.x.

54. Barretina, J., Caponigro, G., Stransky, N., Venkatesan, K., Margolin, A.A., Kim, S., Wilson, C.J., Lehár, J., Kryukov, G.V., Sonkin, D., et al. (2012). The Cancer Cell Line Encyclopedia enables predictive modelling of anticancer drug sensitivity. Nature *483*, 603–607. https://doi.org/10.1038/nature11003.

55. Bae, J.E., Kang, G.M., Min, S.H., Jo, D.S., Jung, Y.K., Kim, K., Kim, M.S., and Cho, D.H. (2019). Primary cilia mediate mitochondrial stress responses to promote dopamine neuron survival in a Parkinson's disease model. Cell Death Dis. *10*, 1–15. https://doi.org/10.1038/s41419-019-2184-y.

56. Shankar, S., Hsu, Z.T., Ezquerra, A., Li, C.C., Huang, T.L., Coyaud, E., Vias, R., Grauffel, C., Raught, B., Lim, C., et al. (2022). A γ-tubulin complex-dependent pathway suppresses ciliogenesis by promoting cilia disassembly. Cell Rep. *41*, 111642. https://doi.org/10.1016/j.celrep.2022.111642.

57. Tian, W.N., Braunstein, L.D., Apse, K., Pang, J., Rose, M., Tian, X., and Stanton, R.C. (1999). Importance of glucose-6-phosphate dehydrogenase activity in cell death. American Journal of Physiology-Cell Physiology *276*, C1121–C1131. https://doi.org/10.1152/ajpcell.1999.276.5.C1121.

58. Pandey, S., Lopez, C., and Jammu, A. (2003). Oxidative stress and activation of proteasome protease during serum deprivation-induced apoptosis in rat hepatoma cells; inhibition of cell death by melatonin. Apoptosis *8*, 497–508. https://doi.org/10.1023/a:1025542424986.

59. Westermann, B. (2010). Mitochondrial fusion and fission in cell life and death. Nat. Rev. Mol. Cell Biol. *11*, 872–884. https://doi.org/10.1038/nrm3013.

60. Youle, R.J., and van der Bliek, A.M. (2012). Mitochondrial Fission, Fusion, and Stress. Science *337*, 1062–1065. https://doi.org/10.1126/science.1219855.

61. Vincent, A.E., Turnbull, D.M., Eisner, V., Hajnóczky, G., and Picard, M. (2017). Mitochondrial Nanotunnels. Trends Cell Biol. *27*, 787–799. https://doi.org/10.1016/j.tcb.2017.08.009.

62. Haapaniemi, E., Botla, S., Persson, J., Schmierer, B., and Taipale, J. (2018). CRISPR–Cas9 genome editing induces a p53-mediated DNA damage response. Nat Med *24*, 927–930. https://doi.org/10.1038/s41591-018-0049-z.

63. Mahadevaiah, S.K., Turner, J.M.A., Baudat, F., Rogakou, E.P., de Boer, P., Blanco-Rodríguez, J., Jasin, M., Keeney, S., Bonner, W.M., and Burgoyne, P.S. (2001). Recombinational DNA double-strand breaks in mice precede synapsis. Nat. Genet. *27*, 271–276. https://doi.org/10.1038/85830.

64. Bellani, M.A., Romanienko, P.J., Cairatti, D.A., and Camerini-Otero, R.D. (2005). SPO11 is required for sex-body formation, and Spo11 heterozygosity rescues the prophase arrest of Atm -/- spermatocytes. J. Cell Sci. *118*, 3233–3245. https://doi.org/10.1242/jcs.02466.

65. Hirano, K., Nonami, Y., Nakamura, Y., Sato, T., Sato, T., Ishiguro, K., Ogawa, T., and Yoshida, S. (2022). Temperature sensitivity of DNA double-strand break repair underpins heat-induced meiotic failure in mouse spermatogenesis. Commun. Biol. *5*, 1–16. https://doi.org/10.1038/s42003-022-03449-y.

66. Gilbert, L.A., Horlbeck, M.A., Adamson, B., Villalta, J.E., Chen, Y., Whitehead, E.H., Guimaraes, C., Panning, B., Ploegh, H.L., Bassik, M.C., et al. (2014). Genome-Scale CRISPR-Mediated Control of Gene Repression and Activation. Cell *159*, 647–661. https://doi.org/10.1016/j.cell.2014.09.029.

67. Konermann, S., Brigham, M.D., Trevino, A.E., Joung, J., Abudayyeh, O.O., Barcena, C., Hsu, P.D., Habib, N., Gootenberg, J.S., Nishimasu, H., et al. (2015). Genome-scale transcriptional activation by an engineered CRISPR-Cas9 complex. Nature *517*, 583–588. https://doi.org/10.1038/nature14136.

68. Xu, D., Cai, Y., Tang, L., Han, X., Gao, F., Cao, H., Qi, F., and Kapranov, P. (2020). A CRISPR/Cas13-based approach demonstrates biological relevance of vlinc class of long non-coding RNAs in anticancer drug response. Sci. Rep. *10*, 1794. https://doi.org/10.1038/s41598-020-58104-5.

69. Li, S., Li, X., Xue, W., Zhang, L., Yang, L.Z., Cao, S.M., Lei, Y.N., Liu, C.X., Guo, S.K., Shan, L., et al. (2021). Screening for functional circular RNAs using the CRISPR–Cas13 system. Nat. Methods *18*, 51–59. https://doi.org/10.1038/s41592-020-01011-4.

70. Pear, W.S., Nolan, G.P., Scott, M.L., and Baltimore, D. (1993). Production of high-titer helper-free retroviruses by transient transfection. Proc. Natl. Acad. Sci. USA *90*, 8392–8396. https://doi.org/10.1073/pnas.90.18.8392.

71. Jainchill, J.L., Aaronson, S.A., and Todaro, G.J. (1969). Murine Sarcoma and Leukemia Viruses: Assay Using Clonal Lines of Contact-Inhibited Mouse Cells. J. Virol. *4*, 549–553. https://doi.org/10.1128/jvi.4.5.549-553.1969.

72. Reid, T.W., Albert, D.M., Rabson, A.S., Russell, P., Craft, J., Chu, E.W., Tralka, T.S., and Wilcox, J.L. (1974). Characteristics of an Established Cell Line of Retinoblastoma2. JNCI. Journal of the National Cancer Institute *53*, 347–360. https://doi.org/10.1093/jnci/53.2.347.

73. Bernstine, E.G., Hooper, M.L., Grandchamp, S., and Ephrussi, B. (1973). Alkaline Phosphatase Activity in Mouse Teratoma. Proc. Natl. Acad. Sci. USA *70*, 3899–3903. https://doi.org/10.1073/pnas.70.12.3899.

74. Rasheed, S., Nelson-Rees, W.A., Toth, E.M., Arnstein, P., and Gardner, M.B. (1974). Characterization of a newly derived human sarcoma cell line (HT-1080). Cancer *33*, 1027–1033. https://doi.org/10.1002/1097-0142(197404)33:4<1027::AID-CNCR2820330419>3.0.CO;2-Z.

75. Biedler, J.L., Helson, L., and Spengler, B.A. (1973). Morphology and growth, tumorigenicity, and cytogenetics of human neuroblastoma cells in continuous culture. Cancer Res. *33*, 2643–2652.

76. Platt, R.J., Chen, S., Zhou, Y., Yim, M.J., Swiech, L., Kempton, H.R., Dahlman, J.E., Parnas, O., Eisenhaure, T.M., Jovanovic, M., et al. (2014). CRISPR-Cas9 Knockin Mice for Genome Editing and Cancer Modeling. Cell *159*, 440–455. https://doi.org/10.1016/j.cell.2014.09.014.

77. Miyoshi, H., Blömer, U., Takahashi, M., Gage, F.H., and Verma, I.M. (1998). Development of a Self-Inactivating Lentivirus Vector. J. Virol. *72*, 8150–8157. https://doi.org/10.1128/jvi.72.10.8150-8157.1998.

78. Zheng, G.X.Y., Terry, J.M., Belgrader, P., Ryvkin, P., Bent, Z.W., Wilson, R., Ziraldo, S.B., Wheeler, T.D., McDermott, G.P., Zhu, J., et al. (2017). Massively parallel digital transcriptional profiling of single cells. Nat. Commun. *8*, 14049. https://doi.org/10.1038/ncomms14049.

79. Davis, M.W., and Jorgensen, E.M. (2022). ApE, A Plasmid Editor: A Freely Available DNA Manipulation and Visualization Program. Frontiers in Bioinformatics *2*.

80. Dehairs, J., Talebi, A., Cherifi, Y., and Swinnen, J.V. (2016). CRISP-ID: decoding CRISPR mediated indels by Sanger sequencing. Sci. Rep. *6*, 28973. https://doi.org/10.1038/srep28973.

81. Martin, M. (2011). Cutadapt removes adapter sequences from high-throughput sequencing reads. EMBnet.journal *17*, 10–12. https://doi.org/10.14806/ej.17.1.200.

82. Sherman, B.T., Hao, M., Qiu, J., Jiao, X., Baseler, M.W., Lane, H.C., Imamichi, T., and Chang, W. (2022). DAVID: a web server for functional enrichment analysis and functional annotation of gene lists (2021 update). Nucleic Acids Res. *50*, W216–W221. https://doi.org/10.1093/nar/gkac194.

83. Vert, J.P., Foveau, N., Lajaunie, C., and Vandenbrouck, Y. (2006). An accurate and interpretable model for siRNA efficacy prediction. BMC Bioinf. *7*, 520. https://doi.org/10.1186/1471-2105-7-520.

84. Klopfenstein, D.V., Zhang, L., Pedersen, B.S., Ramírez, F., Warwick Vesztrocy, A., Naldi, A., Mungall, C.J., Yunes, J.M., Botvinnik, O., Weigel, M., et al. (2018). GOATOOLS: A Python library for Gene Ontology analyses. Sci. Rep. *8*, 10872. https://doi.org/10.1038/s41598-018-28948-z.

85. Pertea, M., Kim, D., Pertea, G.M., Leek, J.T., and Salzberg, S.L. (2016). Transcript-level expression analysis of RNA-seq experiments with HISAT, StringTie and Ballgown. Nat. Protoc. *11*, 1650–1667. https://doi.org/10.1038/nprot.2016.095.

86. Robinson, J.T., Thorvaldsdóttir, H., Winckler, W., Guttman, M., Lander, E.S., Getz, G., and Mesirov, J.P. (2011). Integrative genomics viewer. Nat. Biotechnol. *29*, 24–26. https://doi.org/10.1038/nbt.1754.

87. Schneider, C.A., Rasband, W.S., and Eliceiri, K.W. (2012). NIH Image to ImageJ: 25 years of image analysis. Nat. Methods *9*, 671–675. https://doi.org/10.1038/nmeth.2089.

88. Li, W., Xu, H., Xiao, T., Cong, L., Love, M.I., Zhang, F., Irizarry, R.A., Liu, J.S., Brown, M., and Liu, X.S. (2014). MAGeCK enables robust identification of essential genes from genome-scale CRISPR/Cas9 knockout screens. Genome Biol. *15*, 554. https://doi.org/10.1186/s13059-014-0554-4.

89. Hunter, J.D. (2007). Matplotlib: A 2D Graphics Environment. Comput. Sci. Eng. *9*, 90–95. https://doi.org/10.1109/MCSE.2007.55.

90. van der Walt, S., Colbert, S.C., and Varoquaux, G. (2011). The NumPy Array: A Structure for Efficient Numerical Computation. Comput. Sci. Eng. *13*, 22–30. https://doi.org/10.1109/MCSE.2011.37.

91. Mckinney, W. (2011). pandas: a Foundational Python Library for Data Analysis and Statistics. Python High Performance Science Computer *14*.

92. Ye, J., Coulouris, G., Zaretskaya, I., Cutcutache, I., Rozen, S., and Madden, T.L. (2012). Primer-BLAST: A tool to design target-specific primers for polymerase chain reaction. BMC Bioinf. *13*, 134. https://doi.org/10.1186/1471-2105-13-134.

93. Li, H., Handsaker, B., Wysoker, A., Fennell, T., Ruan, J., Homer, N., Marth, G., Abecasis, G., Durbin, R., and 1000 Genome Project Data Processing Subgroup (2009). The Sequence Alignment/Map format and SAMtools. Bioinformatics 25, 2078–2079. 10.1093/bioinformatics/btp352.

94. Waskom, M.L. (2021). seaborn: statistical data visualization. J. Open Source Softw. *6*, 3021. https://doi.org/10.21105/joss.03021.

95. Wolf, F.A., Angerer, P., and Theis, F.J. (2018). SCANPY: large-scale single-cell gene expression data analysis. Genome Biol. *19*, 15. https://doi.org/10.1186/s13059-017-1382-0.

96. Pedregosa, F., Varoquaux, G., Gramfort, A., Michel, V., Thirion, B., Grisel, O., Blondel, M., Prettenhofer, P., Weiss, R., Dubourg, V., et al. (2011). Scikit-learn: Machine Learning in Python. J. Mach. Learn. Res. *12*, 2825–2830.

97. Virtanen, P., Gommers, R., Oliphant, T.E., Haberland, M., Reddy, T., Cournapeau, D., Burovski, E., Peterson, P., Weckesser, W., Bright, J., et al. (2020). SciPy 1.0: fundamental algorithms for scientific computing in Python. Nat. Methods *17*, 261–272. https://doi.org/10.1038/s41592-019-0686-2.

98. Pertea, M., Pertea, G.M., Antonescu, C.M., Chang, T.C., Mendell, J.T., and Salzberg, S.L. (2015). StringTie enables improved reconstruction of a transcriptome from RNA-seq reads. Nat. Biotechnol. *33*, 290–295. https://doi.org/10.1038/nbt.3122.

99. Li, M., Husic, N., Lin, Y., and Snider, B.J. (2012). Production of Lentiviral Vectors for Transducing Cells from the Central Nervous System. JoVE, 4031. https://doi.org/10.3791/4031.

100. Niedenberger, B.A., and Geyer, C.B. (2018). Advanced immunostaining approaches to study early male germ cell development. Stem Cell Res. *27*, 162–168. https://doi.org/10.1016/j.scr.2018.01.031.

101. Ogawa, T., Aréchaga, J.M., Avarbock, M.R., and Brinster, R.L. (1997). Transplantation of testis germinal cells into mouse seminiferous tubules. Int. J. Dev. Biol. *41*, 111–122.

102. Nishino, K., and Kosako, H. (2022). Immunoprecipitation-Mass Spectrometry for Analysis of Post-Translational Modifications and Interactomes of Target Proteins. Preprint at Proteome Letters. https://doi.org/10.14889/jpros.7.1_9.

103. Miyamoto, T., Hosoba, K., Ochiai, H., Royba, E., Izumi, H., Sakuma, T., Yamamoto, T., Dynlacht, B.D., and Matsuura, S. (2015). The Microtubule-Depolymerizing Activity of a Mitotic Kinesin Protein KIF2A Drives Primary Cilia Disassembly Coupled with Cell Proliferation. Cell Rep. *10*, 664–673. https://doi.org/10.1016/j.celrep.2015.01.003.

104. Onodera, Y., Nam, J.M., Horikawa, M., Shirato, H., and Sabe, H. (2018). Arf6-driven cell invasion is intrinsically linked to TRAK1-mediated mitochondrial anterograde trafficking to avoid oxidative catastrophe. Nat. Commun. *9*, 2682. https://doi.org/10.1038/s41467-018-05087-7.

105. Dickinson, B.C., Lin, V.S., and Chang, C.J. (2013). Preparation and use of MitoPY1 for imaging hydrogen peroxide in mitochondria of live cells. Nat. Protoc. *8*, 1249–1259. https://doi.org/10.1038/nprot.2013.064.

106. Kanatsu-Shinohara, M., Toyokuni, S., Morimoto, T., Matsui, S., Honjo, T., and Shinohara, T. (2003). Functional Assessment of Self-Renewal Activity of Male Germline Stem Cells Following Cytotoxic Damage and Serial Transplantation. Biol. Reprod. *68*, 1801–1807. https://doi.org/10.1095/biolreprod.102.012575.

107. Ge, L., Melville, D., Zhang, M., and Schekman, R. (2013). The ER–Golgi intermediate compartment is a key membrane source for the LC3 lipidation step of autophagosome biogenesis. Elife *2*, e00947. https://doi.org/10.7554/eLife.00947.

STAR★METHODS

KEY RESOURCES TABLE

REAGENT or RESOURCE	SOURCE	IDENTIFIER
Antibodies		
Anti-Plzf antibody	Santa Cruz	Catalog #: sc-28319 Clone: D-9 RRID: AB_2218941
Anti-Sall4 antibody	Santa Cruz	Catalog #: sc-101147 Clone: EE-30 RRID: AB_1129262
Germ cell-specific antigen antibody [TRA98]	Abcam	Catalog #: ab82527 Clone: TRA98 RRID: AB_1659152
Anti-tRFP antibody	Evrogen	Catalog #: AB233 RRID: AB_2571743
Anti-GFP (Green Fluorescent Protein) pAb	MBL	Catalog #: 598 RRID: AB_591819
PerCP/Cyanine5.5 anti-mouse/human CD324 (E-Cadherin) Antibody	BioLegend	Catalog #: 147317 Clone: DECMA-1 RRID: AB_2750305
Alexa Fluor 647 anti-mouse/human CD324 (E-Cadherin) Antibody	BioLegend	Catalog #: 147308 Clone: DECMA-1 RRID: AB_2563955
PE anti-mouse CD117 (c-Kit) Antibody	BioLegend	Catalog #: 105808 Clone: RUO RRID: AB_313217
PE anti-mouse CD147 Antibody	BioLegend	Catalog #: 123707 Clone: OX-114 RRID: AB_2243692
Anti-RD3 antibody	Santa Cruz	Catalog #: sc-390653 Clone: A-9 RRID: N/A
Anti-γ-Tubulin antibody	Sigma	Catalog #: T6557 Clone: GTU-88 RRID: AB_477584
Alexa Fluor 647 Anti-γ-Tubulin antibody - C-terminal	Abcam	Catalog #: ab191114 Clone: TU-30 RRID: AB_2889219
ARL13B Polyclonal antibody	Proteintech	Catalog #: 17711-1-AP RRID: AB_2060867
Alexa Fluor 488 Anti-Tomm20 antibody - Mitochondrial Marker	Abcam	Catalog #: ab205486 Clone: EPR15581-39 RRID: AB_2943509
Anti-α-Tubulin antibody	Santa Cruz	Catalog #: sc-32293 Clone: DM1A RRID: AB_628412
Goat anti-Rat IgG (H + L) Cross-Adsorbed Secondary Antibody, Alexa Fluor 555	Invitrogen™	Catalog #: A-21434 RRID: AB_2535855
Goat anti-Rat IgG (H + L) Cross-Adsorbed Secondary Antibody, Alexa Fluor 647	Invitrogen™	Catalog #: A-21247 RRID: AB_141778
Donkey anti-Mouse IgG (H + L) Highly Cross-Adsorbed Secondary Antibody, Alexa Fluor 488	Invitrogen™	Catalog #: A-21202 RRID: AB_141607

(*Continued on next page*)

Continued

REAGENT or RESOURCE	SOURCE	IDENTIFIER
Donkey anti-Mouse IgG (H + L) Highly Cross-Adsorbed Secondary Antibody, Alexa Fluor 594	Invitrogen™	Catalog #: A-21203 RRID: AB_2535789
Donkey anti-Mouse IgG (H + L) Highly Cross-Adsorbed Secondary Antibody, Alexa Fluor 647	Invitrogen™	Catalog #: A-31571 RRID: AB_162542
Donkey anti-Rabbit IgG (H + L) Highly Cross-Adsorbed Secondary Antibody, Alexa Fluor 488	Invitrogen™	Catalog #: A21206 RRID: AB_2535792
Donkey anti-Rabbit IgG (H + L) Highly Cross-Adsorbed Secondary Antibody, Alexa Fluor 594	Invitrogen™	Catalog #: A-21207 RRID: AB_141637
Biological samples		
C57BL/6JJmsSlc	Japan SLC, Inc.	N/A
Gt(ROSA) 26Sor$^{tm1.1(CAG-cas9*,-EGFP)Fezh}$/J	The Jackson Laboratory (Platt et al.[76])	strain: # 024858
GeCKO v2 Mouse CRISPR Knockout Pooled Library	Sanjana et al.[44]	Addgene: #1000000052 and #1000000053
lentiGuide-Puro	Sanjana et al.[44]	Addgene: #52963
lentiCas9-Blast	Sanjana et al.[44]	Addgene: #52962
lentiGuide-mEGFP	This paper	N/A
lentiGuide-TagRFP	This paper	N/A
lentiGuide-TagBFP	This paper	N/A
lentiGuide-mitoEGFP	This paper	N/A
lentiGuide-sgGcna1-TagBFP	This paper	N/A
lentiGuide-sgRosa26-TagRFP	This paper	N/A
lentiGuide-sgRD3-Puro	This paper	N/A
lenti-shRNA-mEGFP	This paper	N/A
lenti-sh*Ovol2*-mEGFP	This paper	N/A
lenti-sh*Rnf215*-mEGFP	This paper	N/A
lenti-sh*Cldn34c4*-TagBFP	This paper	N/A
lenti-sh*Rd3*-TagBFP	This paper	N/A
lenti-sh*Cebpg*-mEGFP	This paper	N/A
lenti-sh*Rbm26*-mEGFP	This paper	N/A
lenti-sh*P2ry2*-TagBFP	This paper	N/A
lenti-Cldn34c4-HA-P2A-mEGFP	This paper	N/A
lenti-Ovol2-TagBFP	This paper	N/A
lenti-Rd3-HA-P2A-mEGFP	This paper	N/A
lenti-RD3-Spot-P2A-mEGFP	This paper	N/A
pCAG-HIVgp	Miyoshi et al.[77]	RIKEN: RDB04394
pCMV-VSV-G-pRSV-REV	Miyoshi et al.[77]	RIKEN: RDB04393
pCMV-SVF-P2A-VSV-G-pRSV-REV	This paper	N/A
Chemicals, peptides, and recombinant proteins		
Fluo-4 AM	Dojindo	Catalog #: F311
Cell Count Reagent SF	Nacalai	Catalog #: 07553-15
Cellstain- PI solution	Dojindo	Catalog #: F378
Cellstain- DAPI solution	Dojindo	Catalog #: D523
Cellstain- Hoechst 33342 solution	Dojindo	Catalog #: H342
7-AAD Viability Staining Solution	Biolegend	Catalog #: 420404
DRAQ5™	Biostatus	Catalog #: DR50200

(*Continued on next page*)

Continued

REAGENT or RESOURCE	SOURCE	IDENTIFIER
lectin PNA From Arachis hypogaea (peanut), Alexa Fluor™ 647 Conjugate	Invitrogen™	Catalog #: L32460
lectin PNA From Arachis hypogaea (peanut), Alexa Fluor™ 488 Conjugate	Invitrogen™	Catalog #: L21409
Critical commercial assays		
Pre-washed Sterilized Glass Capillary Tubing w/Internal Glass Fiber	Narishige	Catalog #: GDC-1
QIAamp DNA mini kit	QIAGEN	Catalog #: 51304
QuantiFluor ONE dsDNA	Promega	Catalog #: E4871
MegaX DH10B T1R Electrocomp™ cells	Invitrogen™	Catalog #: C640003
MitoPY1	Tocris	Catalog #: 4428
Next Generation Micropipette Puller	SHUTTER INSTRUMENT	Catalog #: P-1000
NEBuilder HiFi DNA Assembly	NEB	Catalog #: E2621
Liberase™ TM	Roche	Catalog #: 5401127001
High-Capacity cDNA Reverse Transcription Kit	Applied Biosystems™	Catalog #: 4368814
TB Green Premix Ex Taq™ II (Tli RNaseH Plus)	Takara	Catalog #: RR820A
HCR™ RNA-FISH Bundle	Molecular Instruments	N/A
Taq DNA Polymerase	Ampliqon	Catalog #: A111103
ChromoTek Spot-Trap Magnetic Agarose	Proteintech	Catalog #: emta-20
Sera-Mag™ SpeedBeads Protein A/G	Cytiva	Catalog #: 17152104011150
4BB™ TruePrime Whole Genome Amplification (WGA) Kit	4basebio[29]	Catalog #: 380100
Deposited data		
Library coverage analysis	This paper	https://doi.org/10.5281/zenodo.10528508
sgRNA library Pool A (input)	This paper	https://doi.org/10.5281/zenodo.10528508
sgRNA library Pool A (1st round)	This paper	https://doi.org/10.5281/zenodo.10528508
sgRNA library Pool A (2nd round)	This paper	https://doi.org/10.5281/zenodo.10528508
sgRNA library Pool B (input)	This paper	https://doi.org/10.5281/zenodo.10528508
sgRNA library Pool B (1st round)	This paper	https://doi.org/10.5281/zenodo.10528508
sgRNA library Pool B (2nd round)	This paper	https://doi.org/10.5281/zenodo.10528508
RD3 interactome data from LC-MS/MS	This paper	ProteomeXchange: PXD042933 Zenodo DOI: https://doi.org/10.5281/zenodo.10528508
Tissue-wide bulk transcriptome dataset	Bgee suite[45]	N/A
Testis RNA-seq data	https://www.refine.bio/samples/SRR823506	Accession: SRR823506
Retina RNA-seq data	Grant et al.[52]	Accession: SRR342458
Testis scRNA-seq data	Hermann et al.[48]	GEO: GSE109033
Retina scRNA-seq data	van Hove et al.[51]	Accession: E-MTAB-9061
Experimental models: Cell lines		
HEK293T	Pear et al.[70]	S. Nagata lab, Osaka Univ RRID: CVCL_0063
NIH3T3	Jainchill et al.[71]	S. Nagata lab, Osaka Univ RRID: CVCL_0594
Y-79	Reid et al.[72]	National Institutes of Biomedical Innovation, Health and Nutrition RRID: CVCL_1893
F9	Bernstine et al.[73]	RIKEN BRC RRID: CVCL_0259
HT-1080	Rasheed et al.[74]	M. Matsuda lab, Kyoto Univ RRID: CVCL_0317
SH-SY5Y	Biedler et al.[75]	Y. Kimura lab, Kyoto Univ RRID: CVCL_0019

(*Continued on next page*)

Continued

REAGENT or RESOURCE	SOURCE	IDENTIFIER
Software and algorithms		
10x Genomics Cell Ranger 6.0.0	Zheng et al.[78]	https://github.com/10XGenomics/cellranger
ApE	Davis et al.[79]	https://jorgensen.biology.utah.edu/wayned/ape/
CRISP-ID v1.1	Dehairs et al.[80]	http://crispid.gbiomed.kuleuven.be
Customized python script for statistical analysis	This paper	https://github.com/SuzukiLab-icems/utils_for_Cell_Genomics_2024
Cutadapt v4.1	Martin et al.[81]	https://github.com/marcelm/cutadapt
DAVID	Sherman et al.[82]	https://david.ncifcrf.gov
docker-cellranger	litd/docker-cellranger	https://github.com/litd/docker-cellranger
DSIR	Vert et al.[83]	http://biodev.cea.fr/DSIR/DSIR.html
FastQC v0.12.1	Babraham Bioinformatics	https://www.bioinformatics.babraham.ac.uk/projects/fastqc/
FlowJo	BD Life Sciences	https://www.flowjo.com
goatools v1.2.4	Klopfenstein et al.[84]	https://github.com/tanghaibao/goatools
guide-caller v1.0.0	This paper	https://github.com/SuzukiLab-icems/guide-caller
HISAT2 v2.2.1	Perțea, M et al.[85]	http://daehwankimlab.github.io/hisat2/
Hub-Explorer v1.0.0	This paper	https://github.com/SuzukiLab-icems/Hub-Explorer
Igv v2.16.1	Robinson et al.[86]	https://software.broadinstitute.org/software/igv/home
ImageJ	Schneider et al.[87]	https://imagej.github.io/software/imagej/
MAGeCK v0.5.9.4	Li et al.[88]	https://sourceforge.net/p/mageck/wiki/Home/
Matplotlib v3.7.0	Hunter.[89]	https://github.com/matplotlib/matplotlib
NIS-Elements Viewer	Nikon	https://www.microscope.healthcare.nikon.com/ja_JP/products/software/nis-elements/viewer
Numpy v1.21.2	van der Walt et al.[90]	https://github.com/numpy/numpy
Pandas v1.5.3	McKinney.[91]	https://pandas.pydata.org
Primer Blast	Ye et al.[92]	https://www.ncbi.nlm.nih.gov/tools/primer-blast/
Proteome Discoverer™ software v2.5	Thermo Scientific	https://www.thermofisher.com
Samtools v1.17	Li et al.[93]	http://www.htslib.org
Seaborn v0.12.1	Waskom.[94]	https://github.com/mwaskom/seaborn
Scanpy v1.9.2	Wolf et al.[95]	https://github.com/scverse/scanpy
Scikit-learn v0.0.post1	Pedregosa et al.[96]	https://github.com/scikit-learn/scikit-learn
Scipy v1.8.0	Virtanen et al.[97]	https://github.com/scipy/scipy
lightSra2Count	This paper	https://github.com/SuzukiLab-icems/Sra2Count/tree/main/lightSra2Count
SRA toolkit v3.0.5	SRA Toolkit	https://hpc.nih.gov/apps/sratoolkit.html
StringTie v2.2.1	Perțea et al.[98]	https://github.com/gpertea/stringtie
TrimGalore v0.6.10	Babraham Bioinformatics	https://www.bioinformatics.babraham.ac.uk/projects/trim_galore/

RESOURCE AVAILABILITY

Lead contact

Further information and requests for resources and reagents should be directed to and will be fulfilled by the lead contact, Jun Suzuki (jsuzuki@icems.kyoto-u.ac.jp).

Materials availability

The plasmids and cell lines generated in this study are available on request to the lead contact.

Data and code availability

The MS proteomics data have been deposited in the ProteomeXchange Consortium via the jPOST partner repository with the dataset identifiers PXD042933. All fastq files and processed proteomics data are deposited to Zenodo repository (https://doi.org/10.5281/zenodo.10528508). All the analysis script including Hub-Explorer is deposited to GitHub repository (https://github.com/SuzukiLab-icems) and Zenodo repository (https://doi.org/10.5281/zenodo.10528508).

EXPERIMENTAL MODEL AND SUBJECT DETAILS

Animals

C57BL/6JJmsSlc mice were purchased from Japan SLC, Inc., and *Gt(ROSA)26Sor*$^{tm1.1(CAG-cas9*,-EGFP)Fezh}$*/J* mice were purchased from Jackson Laboratory (JAX: 026179). Mice were housed at 5 mice per cage and maintained in a temperature- (25 ± 2°C) and humidity- (50 ± 10%) controlled conventional animal room under a 12 h light/dark cycle with unrestricted access to food and water at the Institute for Integrated Cell-Material Sciences (iCeMS), Kyoto University. All animal studies were conducted according to the Regulations on Animal Experimentation at Kyoto University based on the International Guiding Principles for Biomedical Research Involving Animals. Furthermore, the Animal Experiment Committee of Kyoto University approved all procedures employed in the present study (Permission Number: 49-4).

Cell lines

HEK293T and NIH3T3 cells were gifted from Dr. Shigekazu Nagata (Osaka University). Y-79 and F9 cells were acquired from the National Institutes of Biomedical Innovation, Health and Nutrition, and RIKEN BRC, respectively. HT-1080 and SH-SY5Y cells were gifted from Dr. Michiyuki Matsuda (Kyoto University) and Dr. Yasuhisa Kimura (Kyoto University), respectively. Cells were cultured in DMEM media (Wako) with 1% Penicillin Streptomycin (PS) solution (Nacalai) and 10% Fetal Bovine Serum (FBS) (Gibco). Y-79 cells were cultured in RPMI media (Wako) with 1% PS and 20% FBS. SH-SY5Y cells were cultured in DMEM/Ham's F-12 media (Nacalai) with 1% PS and 10% FBS. Each cell line was maintained in a 37°C, 5% CO_2 incubator. For proteomics study in Figure 5, Y-79 *RD3* knockout (*RD3*$^{-/-}$) cells and Spot-tagged RD3 expressing (RD3-Spot) cells were utilized. RD3-Spot cells were established by restoring Spot-tagged RD3 expression in *RD3*$^{-/-}$ cells. The Spot-tagged *RD3* sequence was designed to delete the PAM sequence corresponding to the sgRD3 target site with the mutagenesis primer set described in Table S1 by PrimeSTAR MAX DNA polymerase (Takara).

Plasmid construction

For constructing Sendai Virus Fusion (SVF) protein-containing lentivirus packaging plasmid (pCMV-SVF-P2A-VSV-G-pRSV-REV), the SVF-full length coding sequence (GenBank: U86411.1) with the P2A sequence was synthesized and obtained from Sangon Biotech, then inserted into a pCMV-VSV-G-pRSV-REV plasmid acquired from RIKEN[77] by In-Fusion HD Cloning Kit (Takara) (Figure S1D). To construct lenti-shRNA-mEGFP, the sgRNA scaffold sequence was removed from the lentiGuide-mEGFP plasmid (derived from lentiGuide-Puro[44]) using PrimeSTAR Max DNA Polymerase. The shRNA was designed following RIKEN's protocol (https://dnaconda.riken.jp/Form_PDF/IntRNAien.pdf). All sequences of sgRNA/shRNA oligo and cloning primers used in this study are listed in Table S1.

METHOD DETAILS

Lentivirus production

Lentivirus production was performed according to Li et al.[99] and RIKEN's protocol (https://dnaconda.riken.jp/Form_PDF/IntPrepen.pdf). HEK293T cells were seeded onto sixteen 10 cm culture dishes (Nunc) at 4×10^6 cells/dish. After 24 h incubation, the medium was changed to 5 mL fresh medium without PS and FBS, and incubated for an extra 1 h at 37°C, 5% CO_2. Transfection was conducted by the calcium phosphate precipitation method. In brief, the plasmid mixture was prepared by mixing 272 μg target plasmid, 160 μg pCAG-HIVgp, and 160 μg pCMV-SVF-P2A-VSV-G-pRSV-REV, and made up to 7,200 μL with DDW. Next, 800 μL of 1 M $CaCl_2$ (Wako) was applied to the bottom of the tube containing this plasmid mixture and vortexed vigorously for 10 s. Then, 8,000 μL of 2×BBS (50 mM BES (Nacalai), 280 mM NaCl (Wako) and 1.5 mM Na_2HPO_4 (Wako)) buffer was added dropwise to the plasmid mixture while gently mixing. After incubation at RT for 30 min, 1 mL of the plasmid mixture was applied to HEK293T cells, incubated at 37°C, 5% CO_2 for 6 h, and the medium was then changed to fresh medium containing 10% FBS and 9 mM sodium butylate (Wako). After incubation at 37°C, 5% CO_2 for 40–44 h, the supernatants were collected and divided into two 50 mL tubes to remove cell debris by centrifugation (4°C, 900 G, 10 min). Finally, the supernatant was filtered through a 0.45 μm PES filter (Merck Millipore), divided into eight 15 mL tubes by layering onto 1 mL of 20% sucrose (Wako) solution, and centrifuged at 4°C, 15,000 rpm for 4 h with an angle rotor (Hitachi) to pellet the virus. The virus pellet was resuspended with 500 μL chilled HBSS (Nacalai), layered onto the 1 mL of 20% sucrose solution in 1.5 mL tube, and additionally centrifuged at 4°C, 16,000 rpm for 2 h (Hitachi). The centrifuged virus pellet was vigorously resuspended with 90 μL chilled HBSS, separated into 5 μL aliquots, and stored in a −80°C freezer. For confirming SVF protein expression, the virus aliquot was boiled with Sample Buffer containing 2-ME at 95°C for 5 min and applied to SDS-PAGE, followed by Coomassie Brilliant Blue (CBB) staining.

Titer evaluation for the lentivirus encoding fluorescent protein

Titer evaluation was performed, following the LV-MAX Lentiviral Production System USER GUIDE (Gibco, Cat.A35684, Publication No.MAN0017000). First, HT-1080 cells were seeded onto 24 multi-well plates (Nunc) at 3.5×10^4 cells/well. After 4 h incubation, serially diluted virus solutions (0, 1,000, 2,000, 4,000, 8,000, 16,000, 32,000-fold dilution) were applied to cells and incubated at 37°C, 5% CO_2 for an additional 72 h. Next, cells were detached with 0.25% trypsin EDTA (Wako) and analyzed by FACS Lyric (BD) to quantify the percentage of fluorescent protein-positive population. The following formula was used to calculate the infectious titer unit (IFU/ml):

$$\mathrm{IFU}\Big/\mathrm{ml} = \frac{(20(\%)/100)\times 35,000(\mathrm{cells})\times \text{estimated fold dilution(at 20\%)}}{0.5(\mathrm{ml})}$$

An estimated fold dilution at 20% was calculated by the approximate linearization method (by Microsoft Excel) according to infection efficiency values under 20%.

Titer evaluation for the lentivirus encoding puromycin-resistant protein

HT-1080 cells were seeded onto 96 multi-well plates (Nunc) at 7×10^3 cells/well in triplicate following the LV-MAX Lentiviral Production System USER GUIDE. After 4 h incubation, serially-diluted virus solutions (0, 1,000, 2,000, 4,000, 8,000, 16,000, 32,000-fold dilution) were applied to cells, and 10 μg/mL puromycin (InvivoGen) was added the next day. After 72 h incubation, 10 μL Cell Count Reagent SF (Nacalai) was added to each well, incubated at 37°C, 5% CO_2 for around 1 h, and cell viability was quantified by SYNERGY H1 microplate reader (BioTeK) at 450 nm absorbance. The infectious titer unit (IFU/ml) was calculated as described above regarding %cell viability as %infection.

Determination of mice age for virus injection

The VSVg-coated lentiviruses demonstrate limited infectivity in spermatogonia. However, the application of Sendai Virus Fusion protein facilitates the infection of VSVg-coated lentiviruses into male germ cells, including spermatogonia, even in the testes of adult mice.[27,28] In addition, virus infection has to be performed before the initiation of blood-testis barrier formation, at 15 PND. In light of this technical context, our research aimed to optimize the age of mice while considering the following two issues: 1. The number of spermatogonia is maximized. 2. The number of spermatocytes is not increased excessively. Based on these considerations, we determined that the most suitable age for viral injection is at 11 PND.

Capacitation medium

Non-capacitation medium (NCM) was prepared according to RIKEN's protocol (https://mus.brc.riken.jp/ja/wp-content/uploads/manual/IVF_with_frozen_sperm_ver4.pdf) with 101.6 mM NaCl (Wako), 4.7 mM KCl (Wako), 0.4 mM KH_2PO_4 (Wako), 0.2 mM $MgSO_4$ (Wako), 2.78 mM D-Glucose (Wako), 23.3 mM Na-Lactate solution (Wako), 0.34 mM Na-Pyruvate (Wako), 1% Penicillin-Streptomycin (Nacalai), 20 mM HEPES-NaOH (Nacalai) and 3 mg/mL fatty-acid free BSA (Sigma), and finally adjusted to pH 7.4. Capacitation medium (CM) was prepared by adding 4 mM $CaCl_2$ (Wako). In the experiment, CM was mixed with 1 M $NaHCO_3$ solution (final: 50 mM) and diluted with NCM containing sperms to be 2 mM $CaCl_2$ and 25 mM $NaHCO_3$.

Sperm capacitation and flow cytometry analysis

Sperm capacitation was induced according to Xia et al.[23] 500 μL NCM and 400 μL CM were prewarmed at 37°C in different 1.5 mL tubes on a heat-block. Sperms were extracted from the cauda epididymis (8 weeks∼) into 500 μL NCM, mildly mixed, and incubated on a heat block for 5 min. After 5 min incubation, 400 μL supernatant was transferred to the preheated 400 μL CM containing 0.8 μL Propidium Iodide (Dojindo) and 1.6 μL Fluo-4 AM (Dojindo) and mixed mildly, followed by further incubation at 37°C on a heat block for 60 min with the lid open to facilitate sperm reaction. Finally, the capacitated sperms were analyzed by FACS Aria IIIu (BD) with a 100 μm nozzle while kept warm by setting the chamber temperature to 42°C in order to maintain sperm function.

Immunohistochemistry (IHC)

IHC was conducted by referring to Niedenberger et al.[100] Testes were extracted from several mice at the ages indicated in each figure legend, fixed with 4% PFA (Nacalai) in DPBS at 4°C for 3–8 h (∼4 weeks) or overnight (8 weeks∼), embedded in Tissue-Tek O.C.T compound (Sakura Finetek) and stored at −80°C until sectioning. For immunostaining, embedded testes were sectioned by a cryostat (Leica) at 20 μm, washed three times with DPBS (Nacalai), and blocked with Blocking One Histo (Nacalai) at RT for 10 min. In the case of Figure 4G, the section was additionally fixed with 4% PFA in DPBS at RT for 10 min and washed three times before proceeding onto the blocking step. The section was washed three times and applied to antigen retrieval with HistoVT One (Nacalai) at 70°C for 20 min. After washing the section, the primary antibody (see each figure legend) in DPBS (Nacalai) with 0.1% Triton X-100 (Wako), 1% donkey serum (Sigma), 5 mg/mL of Probumin (Merck Millipore), and 0.01% of Proclin 950 (Sigma) was applied, and incubated at 4°C overnight. For a secondary antibody staining, the antibody solution was applied to the washed section and incubated at RT for 2 h. The secondary antibody solution was prepared below: Goat anti-Rat IgG (H + L) Cross-Adsorbed Secondary Antibody, Alexa Fluor 555 (Invitrogen, A-21434, 1:400) for Gcna1 staining, Donkey anti-Rabbit IgG (H + L) Cross-Adsorbed Secondary Antibody, Alexa Fluor 488 (Invitrogen, A-21206, 1:400) for TagBFP and EGFP staining, Donkey anti-Mouse IgG (H + L) Cross-Adsorbed Secondary

Antibody, Alexa Fluor 488 (Invitrogen, A-21202, 1:400) for Rd3 staining. Finally, the section was washed twice and mounted with FluorSave (Merck Millipore), and stored at 4°C until imaging by Nikon Ti Eclipse Confocal Microscope. For Figures S1A–S1C, we aimed to evaluate the infection efficiency at single-cell resolution; hence, we localized EGFP to a specific organelle by employing a mitochondria target signal-fused EGFP.

Testis dissociation

Extracted testes were dissociated with 1.5 mL dissociation buffer (DPBS including 0.2 U/ml Liberase (Roche), 5 U/μL DNase I (Takara), 5 mM $MgSO_4$ (Wako)) at 37°C for 30 min while shaking at 200 rpm. Dissociated testicular cells were pipetted 20 times with 10% FBS and 2 mM EDTA (Wako) and filtered with pluriStrainer 40 μm (pluriSelect Life Science UG & Co.KG). Filtered cells were washed twice with 500 μL DPBS for downstream analysis.

In vivo knockout study by indel analysis

The SVF-encapsulated lentivirus encoding sgRosa26 and TagRFP was purified as described in the 'Lentivirus production' section and introduced into $Cas9^+$ mice testes at 11 PND via the seminiferous tubule. At 21 PND, the testes were extracted and dissociated, following protocols described in the 'Testis dissociation' section and stained with anti-Basigin (Bsg) antibody (Biolegend, 123701, 1:100) on ice for 30 min. Subsequently, Goat anti-Rat IgG (H + L) Cross-Adsorbed Secondary Antibody, Alexa Fluor 647 (Invitrogen, A-21247, 1:400) and DAPI (Dojindo, 1:1,000) were applied to cells, and incubated on ice for 30 min and $TagRFP^+/Bsg^+$ germ cells were sorted by FACS Aria IIIu and genomic DNA (gDNA) was extracted by the QIAamp DNA mini kit (QIAGEN). The Rosa26 region was amplified from the gDNA with PrimeSTAR GXL DNA Polymerase (Takara), sequenced by Sanger sequencing at Eurofins Genomics Japan, Inc and analyzed by CRISP-ID software[80] to detect the indel position. The primer set for PCR is described in Table S1.

In vivo knockout study by Gcna1 knockout analysis

The SVF-encapsulated lentivirus encoding sgGcna1 and TagBFP was introduced into 11 PND $Cas9^+$ mice testes. One week later, dissociated testicular cells were acquired, following protocols described in the 'Testis dissociation' section, fixed with 4% PFA in DPBS at RT for 10 min and permeabilized with chilled 70% EtOH on ice for 30 min as given below: fixed cells were resuspended with 300 μL chilled DPBS, and chilled 700 μL absolute EtOH was layered followed by vigorously vortexing. Cells were washed twice and stained with anti-Gcna1 (Abcam, ab82527, 1:100), Sall4 (Santa Cruz, sc-101147, 1:50), Plzf (Santa Cruz, sc-28319, 1:50), and TagBFP (Evrogen, AB223, 1:100) antibodies at 4°C overnight. After staining with Alexa Fluor 647 (for Gcna1)/Alexa Fluor 488 (for Sall4 and Plzf)/Alexa Fluor 594 (for TagBFP) conjugated-secondary antibodies (Invitrogen, 1:400) and DAPI (Dojindo, 1:1,000), the $Plzf^+/Sall4^+$ population (for Type A Spermatogonia) and the four chromosomes population (for Primary Spermatocytes) were gated. Gcna1 Median Fluorescent Intensity (MFI) was analyzed for knockout evaluation by comparing the uninfected ($TagBFP^-$) and infected ($TagBFP^+$) cells.

Infection efficiency investigation by flow cytometry

The SVF-encapsulated lentivirus encoding TagBFP was introduced into 11 PND $Cas9^+$ mice testes. One week later, testes were extracted, dissociated, and stained with PerCP/Cyanine5.5 anti-mouse/human Cdh1 antibody (Biolegend, 147317, 1:20). After 30 min incubation on ice, $Cdh1^+$ Type A Spermatogonia were gated and analyzed by FACS Aria IIIu to evaluate the percentage of $TagBFP^+$ population.

Scanning electron microscope (SEM)

Sperms were capacitated, following protocols described in the 'Sperm capacitation and flow cytometry analysis' section. As a control, non-capacitated sperms were prepared by incubating sperms without HCO_3^-. Sperms were washed twice with chilled DPBS and fixed with freshly prepared 2% glutaraldehyde and 4% PFA in DPBS solution. After incubation on ice for 1 h, the sperms were washed twice with chilled DPBS, seeded on 0.1% poly-L-lysine coated glass (25φ) at 5×10^5 sperms, incubated until the glass was semi-dried, washed with 6 mL DPBS, applied to post-fixiation with 1% OsO_4 for 2 h, dehydrated, dried, and finally coated with a thin layer of platinum for analysis with a JEOL JSM-7900F scanning electron Microscope (JEOL Tokyo, Japan).

Sperm *in vivo* genome-wide screening library introduction

GeCKO v2 Mouse CRISPR Knockout Pooled Library[44] was separately used as Pool A and B. First, lentivirus encoding each library was purified, following protocols described in the 'Lentivirus production' section, 4–5 μL lentivirus solutions ($0.4–1.4\times10^8$ IFU/ml) were injected into testes via the seminiferous tubules, following Ogawa et al.[101] In brief, a borosilicate glass injection pipette with 1 mm outer diameter, 0.6 mm inner diameter, and 90 mm length (Narishige, GDC-1) was drawn by Next Generation Micropipette Puller (SHUTTER INSTRUMENT) and snapped by a steel micro tweezers to sharpen the glass tips. Finally, the pipette was filled with the virus solutions for injection.

The expected Multiplicity Of Infection (MOI) in this screening system is around 1∼1.5 according to 30–50% infection efficiency in testicular cells. In a conventional CRISPR screening approach, in which sgRNAs are analyzed after performing a one-time screening, 0.3 MOI (single virus infection) is considered appropriate. On the other hand, our "Revival Screening" aims to cover as many sgRNAs

as possible without any omissions during screening and to enrich only essential sgRNAs by repeating the screening process. The combination of repeated screening and statistical analysis reduce the effects of multiple sgRNA integration.

capacitation induction and sorting

Matured sperms were extracted from the cauda epididymis (8–10 weeks), capacitated, following protocols described in the 'Sperm capacitation and flow cytometry analysis' section and analyzed by FACS Aria IIIu with a 100 μm nozzle. The negative population of Fluo-4 AM was determined according to an un-capacitated sperm-derived intensity (see Figures 2C and 2D) and directly sorted into a 5 mL tube containing 280 μL chilled RLT buffer (QIAGEN) while kept warm by setting the chamber temperature to 42°C for maintenance of sperm function. After sorting, the lysates were inverted 20 times, centrifuged at 4°C, 1,000 G for 15 min and stored at −80°C until gDNA extraction. Under this condition, the number of sorted sperms is expected to be 20,000 sperms per testis, and the final volume is 350 μL due to accumulation of the FACS flow solution (70 μL/20,000 sperms).

genome DNA extraction

Frozen lysates were slowly thawed on ice and mixed with 150 mM DTT (Wako), 200 μg/mL Proteinase K (Sigma) and 200 μg/mL RNaseA (Sigma). DTT solution was prepared just prior to use. After incubation at 56°C for 2 h while shaking, samples were vortexed with the same volume of the buffer AL (QIAGEN) for 5–10 s and vigorously shaken with the same amount of absolute EtOH (final: 33%) for 5–10 s. Subsequently, according to the manufacturer's protocol, gDNA was purified by QIAamp DNA mini kit (QIAGEN). In the elution step, gDNA was eluted twice with 50 μL of 70°C pre-warmed DDW and the first and second elusions were combined for the following analysis. Finally, the gDNA was combined in two different tubes (Pool A and Pool B) and applied to QuantiFluor ONE dsDNA system (Promega) to measure the concentration. The concentration of the obtained gDNA was around 68.2 ± 12.4 pg/μL (total average amount: 67.90 ± 10.55 ng per screening) and the estimated viral copy number was 78,492 ± 12,201 copies per screening.

primase-based Whole Genome Amplification (pWGA)

All extracted gDNA was applied to pWGA using the 4BB TruePrime WGA kit (4basebio). This kit leverages the TthPrimPol primase instead of random hexamer oligos to achieve unbiased amplification in terms of DNA copy amount.[29] In this study, for scaling up the gDNA input capacity, an alternative highly-concentrated denaturation buffer (1 M KOH solution (Nacalai)) and neutralization buffer (400 mM HCl (Nacalai) and 600 mM Tris-HCl pH 7.5 (Nippon Gene)) were utilized instead of the manufacturer's prepared buffer. Finally, input was increased from 2.5 μL to 24.7 μL and applied to phi29 polymerase-based isothermal amplification at 30°C for 6 h. The total amount of amplified gDNA product was 300 μg.

library reconstruction

Detailed methods were described by Maruoka et al.[16] In brief, sgRNA regions were amplified by PCR (33 cycles) from the pWGA products with the indicated primer set.

(1) Fwd: GTTTTAAAATGGACTATCATATGC
(2) Rev: TATCCATCTTTGCACCCGGGC

The purified amplicon harboring sgRNA regions were assembled with a SmaI(NEB)- and NdeI(NEB)- digested lentiGuide-TagBFP plasmid by NEBuilder HiFi DNA Assembly (NEB) at 52°C for 1 h, electroporated into MegaX DH10B T1R Electrocomp Cells (Invitrogen), and incubated at 37°C with supplemented Recovery Medium (Invitrogen) for 2 h, followed by expansion on LB agar. After confirming library variety by counting the colonies formed (around 1×10^7 cells), the reconstructed library-encoding plasmid was purified with QIAGEN Plasmid Maxi Kit (QIAGEN).

next generation sequencing

After repeating steps 1–5 for two rounds to enrich sgRNAs of significance, these enriched sgRNAs were amplified by PCR for 15 cycles with the following primers containing an adaptor sequence and sample barcodes ($N_{5\text{-}6}$) of Pool A and Pool B.

Fwd: AATGATACGGCGACCACCGAGATCTACACTCTTTCCCTACACGACGCTCTTCCG
ATCT($N_{5\text{-}6}$)TCTTGTGGAAAGGACGAAACACCG
Rev: CAAGCAGAAGACGGCATACGAGATTCTACTATTCTTTCCCCTGCACTGT

The sample barcodes $N_{5\text{-}6}$ encode TAGCT(N_5) and ATCGAC(N_6). Finally, equal amounts of the purified amplicons were mixed together and sequenced with the Illumina HiSeq2500 platform at Macrogen Japan.

sgRNA coverage analysis

library introduction

The Pool B GeCKO v2 Mouse CRISPR Knockout Pooled Library (containing 62,804 unique guide sequences)[44] was introduced into 11 PND $Cas9^+$ mice testes via seminiferous tubules, following protocols described in the 'Sperm *in vivo* genome-wide screening' section.

testicular cell dissociation and sorting

Three days or one week later, testes were dissociated as described in the 'Testis dissociation' section to prepare the following four samples: 1. Three testes from three days treatment, 2. Nine testes from three days treatment, 3. Three testes from one week treatment 4. Nine testes from one week treatment. Dissociated testicular cells were permeabilized with 70% EtOH on ice for 30 min, washed twice with DPBS containing 5% Probumin (Merck Millipore), 0.1% Donkey Serum (Sigma), and 0.01% of Proclin 950 (Sigma), incubated with anti-Gcna1 (Abcam, ab82527, 1:200) and Plzf (Santa Cruz, sc-28319, 1:50) antibodies at 4°C overnight, washed

twice, and stained with Alexa Fluor 555 (for Gcna1)- and Alexa Fluor 488 (for Plzf)- conjugated secondary antibodies (Invitrogen, 1:400) and DAPI (Dojindo, 1:1,000). The Gcna1^{+}/Plzf^{+} Type A Spermatogonia were gated and sorted by FACS Aria IIIu, following the same procedure as sperm sorting for subsequent gDNA extraction.

genomic DNA extraction and next generation sequencing

Genomic DNA was extracted in the presence of 200 μg/mL Proteinase K (Sigma) and 200 μg/mL RNaseA (Sigma), following protocols described in the 'Sperm *in vivo* genome-wide screening' section. The sgRNA regions were amplified by PCR with the following primers containing an adaptor sequence and four sample barcodes (N_4: CAAG, N_5: TAGCT, N_6: ATCGAC, N_7: GGTACAG)

(1) Fwd: AATGATACGGCGACCACCGAGATCTACACTCTTTCCCTACACGACGCTCTTCCGATCT

(N_{4-7})TCTTGTGGAAAGGACGAAACACCG

(2) Rev: CAAGCAGAAGACGGCATACGAGATTCTACTATTCTTTCCCCTGCACTGT

The purified amplicons were mixed with equal amount and sequenced with the Illumina HiSeq2500 platform at Macrogen Japan.

sgRNA data processing

The sgRNA sequences were readout by our original shell script, named guide-caller v1.0.0 (https://github.com/SuzukiLab-icems/guide-caller) following a general analysis pipeline, including FastQC, Cutadapt,[81] and MAGeCK.[88] In brief, the 20 bp sgRNA sequences were extracted by Cutadapt[81] with two rounds of trimming from 51 bp with the sequences read according to the following parameters: "-u {N_4:28 N_5:29 N_6:30 N_7:31}" for the first trimming, and "-u {N_4:-3 N_5:-2 N_6:-1 N_7:0}" for the second trimming. The trimmed reads were mapped to an annotation list by MAGeCK.[88] In the GeCKO v2 sgRNA library, several sgRNAs are annotated to multiple genes concurrently, for instance genes with family members (ex. *Il11ra1*, *Il11ra2* and *Gm13305*). Therefore, such genes were merged into a single target, and this change was reflected in the annotation list as a modified list for our analysis. Raw count data is deposited in Table S2.

Reverse transcription (RT)-PCR and quantitative RT-PCR (RT-qPCR)

Testis RNA was extracted from dissociated testicular cells using Cas9^{+} mice at different ages (1–8 weeks) by RNeasy Mini Kit (QIAGEN) and converted to cDNA by High-Capacity cDNA Reverse Transcription Kit (Invitrogen) from 1 μg RNA. The cDNA was diluted 20-fold with DDW in 2.5 ng/μL, amplified with the *Rd3*-specific primer set (Table S1) by Ampliqon polymerase (Ampliqon) for 33 and 40 cycles through RT-PCR, and the same amount of cDNA was amplified with the targeted primer sets (Table S1) by TB Green Premix Ex Taq I (Takara) for 40 cycles in RT-qPCR.

shRNA-based small-scaled screening

validation of knockdown efficiency

SVF-encapsulated lentiviruses encoding shRNAs targeting *LacZ*, *Ovol2*, *Rnf215*, *Cldn34c4*, *Rd3*, *Cebpg*, *Rbm26*, and *P2ry2* were applied to the following cells: NIH3T3-Ovol2OE (for sh*Ovol2*), NIH3T3 (for sh*Rnf215* and sh*Cebpg*), F9-Cldn34c4OE (for sh*Cldn34c4*), NIH3T3-Rd3OE (for sh*Rd3*), Ba/F3 (for sh*Rbm26*), and F9 (for sh*P2ry2*). Each knockdown efficiency was evaluated by qRT-PCR.

investigation of shRNA effect on the spermatogenesis

Validated shRNA-encoded lentiviruses were introduced into 10–11 PND Cas9^{+} mice testes via the seminiferous tubule. After 8–10 weeks, testes and cauda epididymis-derived sperms were extracted for analysis. For testes analysis, testes were initially used for testis weight measurement, subsequently dissociated, stained with PE-conjugated anti-mouse Bsg Antibody (Biolegend, 123707, 1:100), 7-AAD (Biolegend, 1:100), and DRAQ5 (Biostatus, 1:200), and finally 7-AAD^{-}/Bsg^{+} living germ cells were used to evaluate infection efficiency based on the population of fluorescent protein-positive cells. For sperm analysis, sperms were capacitated as described in the 'Sperm capacitation and flow cytometry analysis' section. Sperm number was counted from 10 μL sperm solution (from 800 μL total volume), and Fluo-4 AM intensity was quantified by FACS Aria IIIu after 1 h incubation. All raw data were deposited to Table S3.

scRNA-seq data processing

For adult testicular scRNA-seq data analysis, the following data matrices were utilized: GSE109033_AdultMouseBarcode_filtered_matrix.mtx, barcodes.tsv and genes.tsv.[48] For adult retinal scRNA-seq data analysis, deposited fastq file (Accession: E-MTAB-9061[51]) was obtained via ArrayExpress (https://www.ebi.ac.uk/biostudies/arrayexpress) and processed by CellRanger docker image (litd/docker-cellranger) to generate the filtered matrices. These filtered matrices were processed by Scanpy[95] to cells and genes with the following criteria: 1. Cells with less than 500 (testes) or 200 (retina) detected genes 2. Genes with fewer than 3 cells. Finally, cell types were annotated according to consensus markers[48,51] for each cell type (Figures S4A and S4C). Detailed parameters were described in our analysis script (https://github.com/SuzukiLab-icems/utils_for_Cell_Genomics_2024), following the recommended procedure from the developer.

RNA-seq data processing for Rd3 *5′UTR comparative study*

Analysis flow was described in detail in our original shell script, named lightSra2Count (https://github.com/SuzukiLab-icems/Sra2Count/tree/main/lightSra2Count) by utilizing prefetch, fasterq-dump, trim-galore, HISAT2,[85] and Samtools.[93] Briefly, mouse-derived testis (Accession: SRR823506) and retina (Accession: SRR342458[52]) transcriptome SRA files were obtained from the

SRA run selector, converted to fastq file by fasterq-dump, trimmed with an automatic adaptor identification process implemented by trim-galore and finally aligned to the mouse reference genome (mm10) by HISAT2 to generate bam files. The aligned information was visualized as a Sashimi plot by the Igv genome browser.[86]

Hybridization chain reaction fluorescent in situ *hybridization (HCR-FISH)*

The testis section was prepared according to the IHC procedure and applied to the HCR-FISH process according to the manufacturer's protocol from Molecular Instruments. In brief, the section was washed to remove the O.C.T. compound, additionally fixed with 4% PFA in DPBS at RT for 10 min, permeabilized with 0.5% Triton X-100 (Wako) at RT for 1 h, washed three times with 5xSSC buffer (Nacalai) with 0.1% Tween 20 (Biorad), equilibrated with HCR hybridization buffer at 37°C for 1 h, hybridized by manufacturer-designed probes targeting *Acrv1* and *Rd3* (final concentration: 16 nM), and incubated in a humidified chamber at 37°C overnight. The hybridization probes were designed to target multiple spots (maximum: 20 spots). Finally, 10 μL fluorescent probes with identifiers (*Acrv1*: B1-Alexa Flour 594, *Rd3*: B3-Alexa Flour 647) in 600 μL amplification buffer were applied to the section for the chain reaction. After washing out excess probes, lectin PNA (Invitrogen, 1:200) and DAPI (Dojindo, 1:1,000) were applied to the section, mounted with FluorSave (Merck Millipore), and incubated at 4°C overnight. Nikon Ti Eclipse Confocal Microscope was used to image the section.

Mass spectrometry analysis

Immunoprecipitation was performed, following Nishino et al.[102] In brief, *RD3*$^{-/-}$ and RD3-Spot Y-79 cells were seeded onto a 10 cm dish (Nunc) at 5.0×10^7 cells/10 mL medium, incubated at 37°C, 5% CO_2 for 24 h, fixed by adding 27 μL of 37% formaldehyde (Wako) (final: 0.1%), incubated at RT for 10 min, quenched with 1 mL of 1 M Glycine-NaOH pH 7.5 (Nacalai) (final: 100 mM) at RT for 4 min, washed with 10 mL DPBS, divided into 1.5 mL tubes at 1.0×10^7 cells, and stocked at −80°C as a cell pellet. For immunoprecipitation, the cell pellet was lysed by 500 μL RIPA buffer containing 5 μL Protease Inhibitor Cocktail (Nacalai) and 1 μL Benzonase Nuclease (Sigma), incubated at 4°C for 1 h then centrifuged at 4°C, 20,000 G for 10 min to separate the supernatant. A slurry containing ChromoTek Spot-Trap Magnetic Agarose (Chromotek) was washed three times with 500 μL RIPA buffer before 10 μL was added to the supernatant and incubated at 4°C for 2 h. After the incubation, the immunoprecipitated product was washed three times with 300 μL RIPA buffer containing 3 μL of Protease Inhibitor Cocktail (Nacalai), transferred into a new 1.5 mL tube to remove non-specific binding proteins and additionally washed with 300 μL of 50 mM Ammonium Bicarbonate (ABC) buffer. The final products were resuspended with 50 μL of ABC buffer and transferred into a new 1.5 mL tube for LC-MS/MS analysis. Proteins on the beads were digested by adding 200 ng trypsin/Lys-C mix (Promega) and incubating at 37°C overnight. The resulting digests were reduced, alkylated, acidified, and desalted using GL-Tip SDB. The eluates were evaporated and dissolved in 0.1% trifluoroacetic acid and 3% acetonitrile (ACN). LC-MS/MS analysis of the resultant peptides was performed on an EASY-nLC 1200 UHPLC connected to an Orbitrap Fusion mass spectrometer through a nanoelectrospray ion source (Thermo Fisher Scientific). The peptides were separated on a C18 reversed-phase column (75 μm × 150 mm; Nikkyo Technos) with a linear 4–32% ACN gradient for 0–100 min, followed by an increase to 80% ACN for 10 min and a final hold at 80% ACN for 10 min. The mass spectrometer was operated in data-dependent acquisition mode with a maximum duty cycle of 3 s. MS1 spectra were measured with a resolution of 120,000, an AGC target of 4e5, and a mass range of 375-1,500 *m/z*. HCD MS/MS spectra were acquired in the linear ion trap with an AGC target of 1e4, an isolation window of 1.6 *m/z*, a maximum injection time of 35 msec, and a normalized collision energy of 30. Dynamic exclusion was set to 20 s. Raw data were directly analyzed against the SwissProt database restricted to *Homo sapiens* using Proteome Discoverer 2.5 (Thermo Fisher Scientific) with Sequest HT search engine. The search parameters were as follows: (a) trypsin as an enzyme with up to two missed cleavages; (b) precursor mass tolerance of 10 ppm; (c) fragment mass tolerance of 0.6 Da; (d) carbamidomethylation of cysteine as a fixed modification; (e) acetylation of protein N-terminus and oxidation of methionine as variable modifications. Peptides were filtered at a false discovery rate of 1% using the Percolator node. Label free quantification was performed according to the intensities of precursor ions using the Precursor Ions Quantifier node. Normalization was performed such that the total sum of abundance values for each sample over all peptides was the same.

Primary cilia imaging

Primary cilium imaging was performed according to Miyamoto et al.[103] First, SH-SY5Y cells were seeded onto an 8-well culture slide (Invitrogen) at $2.5–5.0\times10^4$ cells per well, incubated at 37°C, 5% CO_2 for 24 h, and ciliogenesis was induced by changing the medium to fresh serum-free medium. After 24 h incubation, cells were fixed with chilled absolute MeOH at RT for 10 min, blocked with Blocking One Histo (Nacalai) at RT for 10 min, stained with anti-ARL13B (Proteintech, 17711-1-AP, 1:400) and γ-Tubulin (Sigma, T6557, 1:500) at 4°C overnight, washed twice, incubated with the Alexa Fluor 488 (for ARL13B)- and Alexa Fluor 594 (for γ-Tubulin)- conjugated secondary antibody (Invitrogen, 1:400) with DAPI (Dojindo, 1:1,000) at RT for 2 h, washed twice, mounted with FluorSave (Merck Millipore), and stored at 4°C until imaging by Nikon Ti Eclipse Confocal Microscope.

RD3 and mitochondria co-localization imaging

SH-SY5Y cells were seeded onto an 8-well culture slide (Invitrogen) at 1×10^4 cells per well, incubated at 37°C, 5% CO_2 for 24 h, fixed with 4% PFA in DPBS at RT for 10 min, blocked with Blocking One Histo (Nacalai) at RT for 10 min, stained with anti-RD3 antibody (Santa Cruz, sc-390653, 1:100) at 4°C overnight, washed twice, stained with anti-mouse Alexa Fluor 647-conjugated secondary antibody (Invitrogen, A-31571, 1:400) at RT for 2 h, washed three times, stained with Alexa Fluor 488-conjugated anti-Tomm20 antibody (Abcam, ab205486, 1:500) and DAPI (Dojindo, 1:1,000) at RT for 1 h, washed twice, mounted with FluorSave (Merck Millipore), incubated at 4°C overnight, and stored at 4°C until imaging by Nikon Ti Eclipse Confocal Microscope.

Mitochondria distribution imaging

Mitochondria distribution imaging was performed, following Onodera et al.[104] First, SH-SY5Y cells (*RD3* wildtype and knockout cells) were seeded onto an 8-well culture slide (Invitrogen) at 5×10^3 cells (for Control) and 1×10^4 cells (for Cilium Induction) per well, and incubated at 37°C, 5% CO_2 for 24 h. Next, ciliogenesis was induced by changing the media for fresh serum-free media, incubated at 37°C, 5% CO_2 for 24 h, fixed by adding formaldehyde (final: 2%) in DPBS at 37°C for 10 min, washed twice, permeabilized with chilled absolute MeOH on ice for 5 min, washed twice, stained with anti-α-Tubulin antibody (Santa Cruz, sc-32293, 1:250) at 4°C overnight, washed twice, stained with anti-mouse Alexa Fluor 594-conjugated secondary antibody (Invitrogen, 1:400) at RT for 2 h, washed three times, stained with Alexa Fluor 488-conjugated anti-Tomm20 antibody (Abcam, ab205486, 1:500), Alexa Fluor 647-conjugated anti-γ-Tubulin antibody (Abcam, ab191114, 1:500) and DAPI (Dojindo, 1:1,000) at RT for 1 h, washed twice, mounted with FluorSave (Merck Millipore), then stored at 4°C until imaging by Nikon Ti Eclipse Confocal Microscope.

MitoPY1 assay

MitoPY1 staining was performed according to Dickinson et al.[105] Briefly, SH-SY5Y cells (*RD3* wildtype and knockout cells) were seeded onto a 6-well culture plate (Nunc) at 1×10^5 cells per well, incubated at 37°C, 5% CO_2 for 24 h, and ciliogenesis was induced. After 24 h ciliogenesis induction, cells were detached with 150 μL Accutase (Nacalai), mixed with 850 μL DPBS, centrifuged at 4°C, 400 G for 5 min, resuspended with 250 μL DPBS containing 10 μM MitoPY1 (Tocris) and 2 μg/mL Hoechst 33342 (Dojindo), incubated at 37°C for 60 min, centrifuged at 4°C, 400G for 5 min, resuspended with 200 μL DPBS, then analyzed by Synergy H1 plate reader (MitoPY1: ex.488 nm/em.527 nm; Hoechst33342: ex.350 nm/em.461 nm). The raw MitoPY1 signal was normalized by Hoechst33342 signal, and multiplied by 1×10^4 for quantification.

Population study of testicular cells

sh*LacZ* or sh*Rd3* was inserted into a lentiviral vector encoding TagBFP and introduced into 11 PND mice testes via the seminiferous tubule. After mice body and testes weight were measured at 5 or 8 weeks, testes were dissociated and 2×10^6 cells were used for antibody staining with PE-conjugated anti-mouse Bsg Antibody (Biolegend, 123707, 1:100), 7-AAD (Biolegend, 1:100), and DRAQ5 (Biostatus, 1:100). For evaluating the Bsg^+ population, $7\text{-}AAD^-/TagBFP^+$ cells were analyzed by FACS Aria IIIu.

Rd3 knockdown study under N-acetyl-cysteine treatment

sh*LacZ* or sh*Rd3* was assembled into a lentiviral vector encoding TagBFP and introduced into 11 PND mice testes via the seminiferous tubule. From 28 PND, 100 mg/kg N-acetyl-cysteine (NAC) was administrated via i.p. every single day. At 8 weeks, testes were analyzed according to the 'Population study of testicular cells' section.

Quantification of lentivirus infection efficiency under Busulfan treatment

Busulfan administration was performed as described in Kanatsu-Shinohara et al.[106] In brief, 0, 15, 30 and 45 mg/kg Busulfan solutions were prepared in DMSO and administrated to 14 PND mice via i.p. administration. Eight days later, mice body and testes were measured. To study the testicular cell population, testes were dissociated and incubated with anti-Gcna1 (Abcam, ab82527, 1:100) and Plzf (Santa Cruz, sc-28319, 1:50) antibodies at 4°C overnight, washed twice, and stained with Alexa Fluor 647 (for Gcna1)- and Alexa Fluor 488 (for Plzf)- conjugated secondary antibodies (Invitrogen, 1:400) and DAPI (Dojindo, 1:1,000). Testicular cell populations indicated in Figures S10D and S10E were quantified by FACS Aria IIIu. For the evaluation of lentiviral infection efficiency, 7.91×10^7 IFU/ml SVF-coated lentiGuide-mEGFP was introduced into testes via seminiferous tubules. Seven days later, testes were dissociated and stained with PE-conjugated anti-mouse Kit Antibody (Biolegend, 105808, 1:100), Alexa Fluor 647-conjugated anti-mouse Cdh1 antibody (Biolegend, 147308, 1:100), 7-AAD (Biolegend, 1:100), and Hoechst33342 (Dojindo, 1:50), and finally analyzed by FACS Aria IIIu.

Fractionation of testicular cell lysate and western blotting

Organelle fractionation from testes was performed according to Ge et al.[107] In brief, 4 testes from 35 to 42 PND mice were dissociated in Liberase, split into two 1.5 mL tubes, and washed twice with chilled 1 mL DPBS, followed by resuspension with 1.0 mL mitochondria isolation buffer (5 mM Tris-HCl (pH 7.5), 1 mM EDTA (pH 8.0), 1 mM DTT, 250 mM sucrose and protease inhibitor cocktail). Subsequently, cell homogenates were prepared by Dounce homogenization (20 times strokes) on ice, subjected to sequential differential centrifugation at 300G, 1,000G, 3,000G, 5,000G, 8,000G and 20,000G at 4°C for 5 min, and lysed with RIPA buffer containing protease inhibitor cocktail, followed by western blotting.

Western blotting was performed in accordance with Maruoka et al.[16] In brief, 20 μg lysates from each fraction were boiled in Sample Buffer containing 2-ME at 95°C for 5 min, applied to SDS-PAGE at 35 mA for 30 min, transferred to a PVDF membrane at 65 mA for 60 min, blocked with PVDF Blocking Reagent for Can Get Signal (TOYOBO), and incubated with anti-RD3 (Santa Cruz, sc-390653, 1:500) and Tomm22 (Atlas Antibody, HPA003037, 1:1,000) antibodies in Can Get Signal Immunoreaction Enhancer Solution 1 (TOYOBO) at 4°C overnight. Next, PVDF membranes were washed three times, incubated with 5,000-fold-diluted HRP-conjugated goat anti-mouse or rabbit Igs (Dako) in Can Get Signal Immunoreaction Enhancer Solution 2 (TOYOBO) at 4°C for 2 h, washed three times and reacted with Amersham ECL Select Western Blotting Detection Reagent (Cytiva), followed by visualization with FUSION chemiluminescence imaging system (Vilber).

QUANTIFICATION AND STATISTICAL ANALYSIS

Quantification and statistical analysis for experimental data

All experiments were performed with biological replicates described in each figure legend. In the shRNA-based small-scale screening, the number of mice was indicated as "n." Outlier removal was only conducted in mass spectrometry analysis. All animal

data were used for analysis. p value was calculated according to an unpaired t test by the Python scipy.stats.ttest_ind function[97] with default parameter. $p < 0.05$ was used as a threshold for evaluation of significance.

Tissue-wide comparative study for characterizing gene expression

Tissue-wide RNA-seq data were downloaded from the Bgee suite[45] in TPM-valued format and filtered into specific mice data containing C57BL/6J mice and C57BL/6J hybrid mice with 129SvEvTac, DBA/2J, and CAST/EiJ. The total dataset was constructed from 20 studies harboring 34 tissues from 252 samples. The dataset information is described in detail in Table S4. For gene expression profiling, all datasets were combined, and the target genes were analyzed by an original Python script (https://github.com/SuzukiLab-icems/utils_for_Cell_Genomics_2024). Finally, each TPM value was converted into Log_2(TPM+1).

Rd3 expression profiling in testicular cells and retinal cells

Testicular and retinal scRNA-seq data were processed as outlined in the 'scRNA-seq data processing' section. The data analysis was executed in several stages: Initially, raw gene counts were transformed into ln(CPM+1) using Python scanpy.pp.normalize_total and scanpy.pp.log1p functions.[95] This transformation was a precursor to the smoothing process by a moving average, which was performed using the scanpy.pl.paga_path function (n_avg = 50),[95] to generate a gene expression matrix. This matrix was then utilized for *Rd3* expression profiling and subsequent analysis with Hub-Explorer. In this process, we integrated every sequential group of 50 neighboring cells into a single cell representation (resulting in a reduction from 6,693 to 6,644 cells for testicular data and from 4,599 to 4,550 cells for retinal data). Accordingly, cell type information was reassigned to each identified cell cluster using Python numpy.floor function.[90] Finally, gene expressions were normalized to a *Z* score across all cell types employing the scipy.stats.zscore function,[97] and visualized in Figures 4C, S4A and S4C.

Analysis for *in vivo* genome-wide screening

sgRNA read counts were summarized as a raw count table (values: read counts/columns: sgRNA IDs/index: gene names) by an original Python script contained in guide-caller v1.0.0 (https://github.com/SuzukiLab-icems/guide-caller/blob/main/v1.0.0/matrix_shaper.py), and every count was converted into Log_2(CPM +1) and an Enrichment Score (ES). The ES was calculated by modifying Log_2FoldChange formula so that detected and undetected sgRNAs are precisely distinguished while maintaining correlation between Log_2FoldChange and ES at the significant region (Log_2FoldChange $\geqq 1.5$). This score was calculated by comparing the test data (test) to control data (ctrl) as described below:

$$\text{Enrichment Score (ES)} = \text{Log}_2\left(1 + \frac{\text{CPM(test)}}{\text{CPM(ctrl)}+1}\right)$$

The correlation between ES and Log_2FoldChange was validated in Figures S2G and S2H. The analysis script was deposited to GitHub repository (https://github.com/SuzukiLab-icems/utils_for_Cell_Genomics_2024).

Analysis for library coverage investigation

The sgRNA read count table was generated, following protocols described in the 'Analysis for *in vivo* genome-wide screening' section, and every read count was converted into Log_2(CPM+1) and shown as a cumulative plot by the Python seaborn.ecdfplot function.[94] The analysis script was deposited to the GitHub repository (https://github.com/SuzukiLab-icems/utils_for_Cell_Genomics_2024).

To evaluate the cumulative count of the nine testes-derived sgRNAs at day three (Figure 2A, coverage = 73.5%, total count of detected sgRNA = 44,518), 35,334 sgRNAs were detected over 29.78 counts (which satisfy Log_2(CPM+1) = 2, *total sgRNA counts = 9,926,238) (79.4%), that we considered as the threshold for a valid count of sgRNAs. According to this criterion, we evaluated the number of genes and total sgRNA counts. As a result, we confirmed that there was no biased count of most of the sgRNAs based on the equal distribution around 2–8 Log_2(CPM+1) (Figures S2A and S2B). From these data, we determined that sgRNA coverage was sufficient for screening. Further analysis showed that over half of the genes were targeted by more than two sgRNAs (each gene is targeted by three sgRNAs) in Type A Spermatogonia's genome from nine testes, but not three testes, at day three and one week (Figures S2C and S2D).

Hub-Explorer

The analysis package was deposited to the GitHub repository with detailed analysis flow (https://github.com/SuzukiLab-icems/Hub-Explorer). In brief, this analysis proceeded as described below.

1. Generation of the cell-type specific gene co-expression (GCN) network:

According to the input expression matrix from scRNA-seq data, the Spearman correlation coefficient between targets and every gene was calculated by the Python scipy.stats.spearmanr function[97] in a multiprocessing manner to extract highly-correlated pairs above Spearman's $\rho = 0.8$ as the gene co-expression network (GCN) for each target.

2. Hub components identification and back-annotation to target genes:

Each GCN was applied to gene ontology (GO) analysis iteratively using goatools[84] to extract significant GO terms (BH_FDR<0.05) as hub components, and these hub components were back-annotated to the targets.

3. Similarity-based K-means clustering for core signaling hub identification:

The Jaccard Similarity Index was calculated as described below for evaluating similarity among targets according to the hub components:

$$\text{Jaccard Similarity Index (target A, target B)} = \frac{|\text{target A} \cap \text{target B}|}{|\text{target A} \cup \text{target B}|}$$

Finally, the Python sklearn.cluster.KMeans function[96] was utilized to cluster the targets according to the Jaccard Similarity Index, and the overlapping hub components were extracted as the core signaling pathway. As a benchmark for the K-means method, a dendrogram-based clustering was conducted and labeled on the Jaccard Similarity Index-based clustermap by the Python seaborn.clustermap function.[94]

Mass spectrometry analysis for profiling RD3 interactors

Three replicates were analyzed in each sample from *RD3*$^{-/-}$ and RD3-Spot Y-79 cells. Raw spectra data were processed by Proteome Discoverer 2.5 (Thermo Scientific) to generate a normalized signal intensity table, and the original Python script removed outlier values according to the Z test-based approach (https://github.com/SuzukiLab-icems/utils_for_Cell_Genomics_2024) below p value = 0.01. This script could detect high outliers from the *RD3*$^{-/-}$ cells-derived data and a low outliers from the RD3-Spot cells-derived data for enhancing detection sensitivity. Subsequently, Log_2FoldChange was calculated by dividing the signal intensities of RD3-Spot cells by those of *RD3*$^{-/-}$ cells, and the p value was determined from the Python scipy.stats.ttest_ind function[97] following unpaired t test. Finally, RD3 interactors were extracted according to Log_2FoldChange $\geqq$ 1.5 and p value < 0.05 (Table S5).

Testicular cell identification highly expressing Rd3 interactors

The 269 candidate proteins obtained in Figure 5A were clustered according to testicular cell expression pattern. A detailed analysis script was deposited to the GitHub repository (https://github.com/SuzukiLab-icems/utils_for_Cell_Genomics_2024). In brief, gene expression data of these 269 proteins were acquired from testis scRNA-seq data used in Figures 4 and 5 and converted into a *Z* score from ln(CPM+1) by the Python scipy.stats.zscore function.[97] The following formula was utilized to identify the cell type highly expressing each of the 269 genes:

$$\text{Cell Type Index (CTI)} = \text{Z-score}\left(\text{Cell Type}_{i(1 \leq i \leq N)}\right) - \frac{\left(\sum_{k=1}^{N} \text{Z-score}(\text{Cell Type}_k)\right) - \text{Z-score}(\text{Cell Type}_i)}{\text{Number of Cell Types (N)} - 1}$$

According to the CTI value, 269 genes were categorized into a specific group above CTI = 0.98, and the number of assigned groups was summarized and counted (Figure 5C, and Table S6).

Gene ontology (GO) analysis

The mouse- and human-derived Ensembl IDs of targeted genes/proteins were applied to DAVID software,[82] analyzed in the GOTERM_DIRECT categories and filtered into significant GO terms below a p value described in each figure legend.

Mitochondrial distribution analysis

Mitochondrial distribution was quantified, following Onodera et al.[104] by MetaMorph software (Molecular Devices) with the originally developed macro program as the journal function in this software. In brief, fluorescent images of nuclei (DNA), mitochondria (Tomm20), microtubule (α-Tubulin), and microtubule organizing center (MTOC: γ-Tubulin) were loaded to automatically or manually determine the thresholds for detecting Tomm20 and α-Tubulin fluorescent signal. In the manual determination, Tomm20 signal intensity was adjusted to be the most sensitive while removing background noise. This manual adjustment was repeated twice, and the same result was confirmed. The selected single cells were applied to automatic alignment with γ-Tubulin staining (MTOC), and boundaries of the intracellular regions (#1 to #5) were generated. Finally, the Tomm20 fluorescence signal intensity was measured at each region, and converted into the density score by calculating the ratio comparing signal intensities among each region (Figure S6B).

Ciliogenesis evaluation

Primary cilium was distinguished with a co-stained pattern of γ-Tubulin and ARL13B. As technical replicates, ten sections were acquired per sample, and the cilium length and number of cilia were measured by Nikon NIS-Elements software. Finally, these experiments were performed three times as biological replicates to quantify the population of ciliary cells and length of induced cilia. The cilium frequency was calculated by dividing the number of primary cilia by the total number of cells.